Arabian Journal of Geosciences
September 2012, Vol. 5 (5), Pages 903-924
http://dx.doi.org/10.1007/s12517-011-0476-3

The Cryogenian arc formation and successive high-K calc–alkaline plutons of Socotra Island (Yemen)

Y. Denèle[1, 2, a, *], S. Leroy[1], E. Pelleter[3], R. Pik[4], J-Y. Talbot[5], K. Khanbari[6]

[1] UPMC Univ Paris 06, UMR 7193, ISTEP, 75005 Paris, France
[2] Géosciences Montpellier, UMR CNRS 5243, Université Montpellier II, Place Bataillon, 34095 Montpellier, France
[3] IFREMER, Centre de Brest, BP70, 29280 Plouzané, France
[4] CRPG, Nancy-Université CNRS, 54501 Vandoeuvre-lès-Nancy, France
[5] CREGU, 54501 Vandoeuvre-lès-Nancy, France
[6] Geological Survey, Sanaa, Republic of Yemen

[a] Present address : GET, Université de Toulouse-CNRS-IRD-OMP, 14 Avenue E. Belin, 31400 Toulouse, France

*: Corresponding author : Yoann Denèle, email address : yoann.denele@get.obs-mip.fr

Abstract:

The Socotra Island belongs to the southern rifted margin of the Gulf of Aden and occupied in Neoproterozoic times a key position to constrain the age and the nature of the largely hidden Neoproterozoic rocks of the Arabian plate. Our integrated field, petrographic, geochemical and geochronological study in the Neoproterozoic rocks recognises three main successive events: (a) high-temperature ductile deformation and metamorphism forming probably in a compressive or transpressive regime; (b) mafic to intermediate intrusions as vertical sheets, kilometre-scale gabbro laccoliths, mafic dike swarm and lavas which present mainly a depleted arc signature with some evidences of evolution from an enriched-arc signature; (c) felsic intrusions mainly composed of highly potassic calc–alkaline and pinkish granites dated between 840 and 780 Ma. Relationships between the various petrographic types and U–Pb data suggest that these events occurred during a relatively short time span (80 Ma at max). Earlier high-temperature–low-pressure metamorphism stage as well as geochemical signature of mafic rocks show that development of Cryogenian formations of Socotra were controlled successively by an Andean-arc and a back-arc setting. These features cannot be easily reconciled with those of the Arabian–Nubian shield to the west of Socotra and of the Mozambique Belt to the south. We propose that the Socotra basement was developed at an active margin close to the India block in Cryogenian times.

Keywords : Neoproterozoic ; East African–Antartic Orogen ; Arabian–Nubian shield ; Socotra Island ; Andean-type arc ; Back-arc basin

1. Introduction

The East-African-Antartic-Orogen (EAAO, Fig. 1a), one of the hugest orogen of the Earth history, extends over 8000 kilometres from Egypt to the north to Antarctica to the south (Stern, 1994; Meert, 2003; Jacobs and Thomas, 2004, 2010). The EAAO corresponds to a N52 S Neoproterozoic collision zone between proto-East Gondwana represented by the current Arabia, Somalia, Pakistan, India and Madagascar and the proto-West Gondwana represented by the East-Saharian, Congo and Tanzania cratons (Meert, 2003; Collins and Pisarevsky, 2005; Collins, 2006). This orogen presents a great complexity due to the fact that East and West Gondwana did not exist as Neoproterozoic supercontinents in their own right, but correspond to an accretion of various terranes which gathered during the Neoproterozoic time (see Collins and Pisarevsky, 2005, and references therein). The northern part of the EAAO corresponds to the Arabian-Nubian shield (ANS, Fig. 1b) dominated by juvenile mid-Neoproterozoic (Cryogenian) island-arc terranes associated to microcontinental blocks such as the Afif-Abbas composite terrane and the Al Mahfid gneiss terrane (e.g. Stern, 1994; Whitehouse et al., 1998 and 2001; Johnson and Woldehaimot, 2003, Meert, 2003; Collins and Pisarevsky, 2005), both bounded by sutures zones with ophiolites. ANS is characterized by mild accretion at low to medium metamorphic grade (Stern, 1994; Shackleton, 1996) which occurred between 700 and 600 Ma (Nehlig et al., 2002, references therein), and by a final stage of post-orogenic extension marked by late calc-alkaline and alkaline igneous activity and by formation of some core complexes (Blasband et al., 2000; Greiling et al., 1994; Avigad and Gvirtzman, 2009) which began around 600 Ma (Jonhson and Woldehaimot, 2003). By contrast the southern part of the EAAO shows high-grade rocks

of Ediacaran-early Cambrian age and is devoid of accreted juvenile Neoproterozoic arc formations (Jacobs and Thomas, 2004, Bingen et al., 2009). This part of the orogen seems to represent a continent-continent collision zone which occurred during the final accretion of various Gondwana blocks (Muhlongo and Lenoir, 1994; Jacobs et al., 1998; Kröner et al., 2001, Jacobs and Thomas, 2004).

There is a lack of magnetic data for the period between 1 Ga to 820 Ma to identify clearly the eastern limit of the EAOO and of the composites terranes of the ANS (Li et al., 2008). For instance, new models of late Mesoprotezoic reconstruction proposed that the ANS microcontinental blocks were either placed adjacent to northeast India (e.g. Li and Powell, 2001), adjacent and outboard of the Congo-São Francisco cratons (Collins and Pisarevsky, 2005), or between India and Sahara (Li et al., 2008). The Socotra Island (Yemen, Fig. 1b) have occupied, prior to the Oligo-Miocene Gulf of Aden opening (e.g. d'Acremont et al., 2006; Leroy et al., 2010a), a key position between the proto-East Gondwana, the high-grade rocks of the EAAO and the ANS (Fig. 1a). It corresponds, together with the basement of Mirbat in Oman, to the only km-scale outcrop of Neoproterozic rocks in the eastern part of the Arabic plate (Fig. 1b). In this way, the study of the Socotra Neoproterozoic rocks should allow the specification of the boundaries of the various domains of the EAAO and their geological histories. We investigate the Neoproterozoic basement of Socotra and propose, based on an integrated field, petrographic, geochemical and geochronological study, that it corresponds to a well-preserved Cryogenian arc that may have formed above an active margin of the Indian proto East-Gondwana block.

Geological setting

The Socotra Island belongs to the southern rifted margin of the Gulf of Aden which is an active oceanic basin (Leroy et al., 2004). The Gulf of Aden forms by the split away of Somalia plate to the South and Arabian plate to the North resulting from an oblique rifting characterized by a N20°E-striking extension and a N70°E-oriented rift (Bellahsen et al., 2006; Autin et al., 2010). Rifting history started around 35 Ma and oceanic accretion is recorded since 17.6 Ma along the whole Gulf of Aden, sensu stricto (e.g. Leroy et al., 2010a and b; Leroy et al., this volume).

The Gulf of Aden rifting is expressed in two different ways in the Socotra Island: a western domain made up of two well-expressed Oligo-Miocene tilted blocks (Razin et al.,

104 2010; Fig. 2) and an eastern domain composed of a single and huge tilted block formed by the
105 Haggier 1500 m-high mountains (Fig. 2). These two domains are separated by a NE-SW
106 transfer fault zone dipping toward the northwest. The hanging wall of the transfer zone
107 corresponds to the tilted blocks bounded by N110°E normal faults and possess a Quaternary
108 relief lower than the footwall which is the main basement outcrop of the Island (Fig. 2).
109 Three main basement outcrops can be observed in the island (Fig. 2), which correspond
110 to three basement highs located at the head of tilted blocks. The Qalansya and the Sherubrub
111 areas are located in the western part of the island and both represent respectively *ca.* 65 km^2
112 and 50 km^2. The most voluminous basement outcrop, the Mont-Haggier basement high
113 representing *ca.* 580 km^2 is located at the eastern part of the island. The Neoproterozoic
114 basement of Socotra displays a great variety of metamorphic, plutonic and volcanic rocks
115 previously studied by Beydoun and Bichan (1970). They have evidenced that the oldest part
116 of this basement is made of amphibolite facies meta-sediments and meta-igneous rocks which
117 have been intruded by synkinematic granites and late-kinematic gabbros. Post-kinematic
118 igneous activity gave rise to a sequence of volcanic rocks, hornblende/biotite and peralkaline
119 granites, gabbros and minor intrusions, which make up the bulk of the Haggier mountains. At
120 the footwall of the major tranfer fault of Socotra, Beydoun and Bichan (1970) have evidenced
121 an association of bedded mudstones, sandstone and tuffs belonging to the Hadibo series.
122 Beydoun and Bichan (1970) proposed that: (i) metamorphic events and synkinematic plutonic
123 rocks are Precambrian in age, (ii) the Hadibo series is late pre-Cambrian, and (iii) the
124 peralkaline granites are Early Paleozoic.
125 The reconstruction of the Gulf of Aden shows that the Socotra Island has occupied, prior
126 to the Oligo-Miocene rifting, a position close to the Precambrian Mirbat and Al Halaaniyat
127 Islands outcrops in Oman (Figs. 1b, e.g. d'Acremont et al., 2006; Leroy et al., 2010a). Gass et
128 al. (1990), based on few geochemical and Rb/Sr whole-rock ages ranging from 850 ± 27 Ma
129 to 706 ± 40 Ma, proposed that Precambrian rocks of Oman lie within the Pan-African domain
130 *s.l.* and are not part of an older basement such as that identified in eastern Saudi Arabia (Afif
131 and Al-Mahfid Terranes, Fig. 2b). Mercolli et al. (2006) defined four units in the
132 Neoproterozoic basement of Mirbat. The Juffa group corresponds to alternation of
133 paragneisses, amphibolites and few meta-ultramafic lenses. U-Pb ages on zircon and Pb-Pb
134 ages on garnet clustering around 815 Ma are interpreted as the age of the metamorphism in
135 amphibolite facies (Mercolli et al., 2006). The Sadh Group corresponds to two types of
136 orthogneisses dated by U-Pb *in situ* method on magmatic looking zircons at 816 ± 12 Ma and
137 799 ± 5 Ma (Mercolli et al., 2006). The Tonalite Group including three kilometre-scale calc-

alkaline plutons was dated by U-Pb *in situ* method around 780-790 Ma (Mercolli et al., 2006). Finally, the Granite Group comprises: (i) different types of dikes and small bodies of granite dated by step leaching Pb/Pb on garnet between 770 and 750 Ma, (ii) two small granitic plutons without precise ages, (iii) basaltic to rhyolitic Shaat Dike Swarm without precise age.

Petrographic and microstructural study of the Socotra basement

The Neoproterozoic basement of Socotra displays a great variety of metamorphic, plutonic and volcanic rocks. A preliminary map of the various lithological formations was performed by Beydoun et al. (1970). We have completed and modified this map for the three principals inliers of Neoproterozoic rocks by field study and satellite images (Fig. 2 and 3). This section describes the different lithological formations of the Socotra basement.

The metamorphic basement

The metamorphic basement corresponds to an alterning of quartzites, paragneisses, micaschists, orthogneisses and ortho-amphibolites. Paragneisses and red or white quartzites crop out on large kilometre scale area. Orthogneisses and ortho-amphibolites are observed as metre to hectometre-scale lenses (Fig. 4a) or boudins in paragneisses and quartzites. Finally micaschists are only locally observed.

Micaschists consist of quartz, biotite, muscovite and locally andalusite. Paragneisses display paragenesis of quartz, alkali feldspar, plagioclase, biotite, muscovite, sillimanite and locally relictual andalusite (Fig. 4b). These two-micas micaschists and paragneisses seem to be derived from the same metapelitic protolith affected by different grades of metamorphism. Paragneisses show frequently evidences of partial melting and correspond to metatexites (Fig. 4b), with 30 % max. of leucosomes. In two areas migmatites are strongly evolved and correspond to diatexites (e.g. Menhert, 1968), which contain an important amount of cordierite. Orthogneisses are composed mainly by porphyric alkali feldspar, quartz and biotite (= augengneisses). Amphibolites correspond to former sills of mafic rocks (Fig. 4a), probably gabbros as shown by observations of relictual orthopyroxene and plagioclase laths (Fig. 4c), affected by a HT-LP metamorphism with neo-formation in the amphibolite-facies of Hb+Ep+Ab and coeval deformation.

Rocks of the metamorphic basement show a well-defined foliation associated to multi-scale folding. Foliations and contact between the different metamorphic formations are generally steeply dipping and oriented on average at *ca.* N80°E. Syn-kinematic neo-formed sillimanite which replaces andalousite observed as relic in paragneisses (Fig. 4b), and spectacular anatexis phenomena with leucocratic/melanocratic banding paralell to the foliation show that an important HT-LP metamorphism under amphibolite facies conditions affected the oldest rocks of Socotra during the main deformation event.

The volcanic series

To the south of the Mont-Haggier area the metamorphic unit is overlain by an association of pyroclastic and effusive rocks belonging to the Southern Haggier volcanic series. Contact between these two units is subhorizontal and devoid of evidence of deformation. The effusive rocks correspond to an alterning of rhyolitic, andesitic, dacitic and basaltic lavas. Pyroclastic rocks, together with thin lava flows, are mainly located to the west of the volcanic formation (Beydoun and Bichan, 1970) and show an alternation of breccias (Fig. 4d), agglomerates, and tuffs (Fig. 4e). Although volcanic rocks are devoid of evidence of deformation and of large metamorphism overprint, we observed locally at the base of the volcanic complex some evidences of HT metamorphic overprint marked by replacement in basaltic lava of pyroxene minerals by hornblende.

At the footwall of the transfer fault, close to Hadibo, we have observed very peculiar yellowish basalt (sample SP15A, localization in figure 2) with a doleritic texture. This basalt (Fig. 4f) is intruded by the Haggier pink granite (see below). Relationships between this basalt and the Southern-Haggier volcanic series are difficult to determine.

The mafic to intermediate plutonic sheets

To this group belong several hectometre to metre thick sheets of tonalites, granodiorites and diorites that have intruded the metamorphic basement in Qalansya, Haggier and Sherubrub areas, and that were successively deformed under amphibolite facies conditions.

We studied in detail this group in the western part of the Qalansya basement high, where we observed on a hundred metres long banks along the road, several sheets of more or less differentiated plutonic rocks on a short distance (Fig. 5A). Petrographically fine-grained tonalites and medium to coarse-grained granodiorites are composed of 30 to 40 % of plagioclase, 30 to 40 % of quartz, 10 to 25 % of alkali felspar and 10 % of mafic minerals

(green hornblende and biotite). We have observed also magnetite, zircon, apatite and sphene. Diorites are fine to medium-grained and composed of 40 to 60 % of plagioclases, 30 to 40 % of green hornblende. We have observed also quartz and accessory minerals corresponding mainly to magnetite, allanite, zircon, apatite and sphene. Locally these rocks are affected by intense metamorphic recrystallization under amphibolite facies conditions as shown by the growth of secondary hornblende, albite and epidote (Figs. 5 B-a and B-b).

Emplacement of diorites, tonalites and granodiorites occurred probably by successive pulses as shown by the sharp contacts between the different sheets of these rocks (Fig. 5 B-c and B-d). We observed also sometimes mingling between diorites and granodiorites suggesting that emplacement of successive pulses occurred rapidly (Fig. 5 B-e). These diorites and granitoids display a discrete steeply dipping foliation oriented N80°E and a subvertical stretching lineation marked by disposition of neo-formed hornblende grains along their long axis (Fig. 5 B-b and B-f). Dikes of microgranite, aplite and basalt have later intruded the sheets of mafic to intermediate plutonic rocks.

The layered gabbros

Two km-scale bodies of layered gabbros occur in Socotra. The Haggier layered gabbros intruded the metamorphic basement, covers *ca.* 40 km^2 of low rusty-looking hills to the E-SE of Hadibo. These gabbros are devoid of any solid-state deformation and present a magmatic layering (Fig. 6a) with a rhythmic alternation of pyroxene and plagioclase-rich layers. These layers vary from a few millimetres, where individual bands can be traced over a distance of several metres, to several centimetres in thickness. Petrographically, medium to coarse-grained gabbros show a cumulate texture and consist of 60 to 80 % of zoned labradorite and 40 to 20 % of mafic minerals (Fig. 6b). Mafic minerals consist of clinopyroxene, orthopyroxene and more rarely olivine replaced by hornblende and locally by chlorite and tremolite-actinolite that attests that a middle grade metamorphic event, followed by a low-grade event, have affected these gabbros. Accessory minerals correspond mainly to magnetite.

The Sherubrub gabbros cover a surface of *ca.* 6 km^2 in the western part of the area and show the same petrographic characteristics as the Haggier layered gabbros. These gabbros are locally associated with intermediate rocks as tonalites and granodiorites and present magmatic layering (Fig. 6c and d).

238

239 *Granites*

240

241 Two kilometre-scale bodies of granitic rocks crop out in Socotra: the Sherubrub pluton
242 and the Mont-Haggier pluton.

243 The Sherubrub pluton and its satellites cover half the Sherubrub area on *ca.* 25 km^2. It is
244 made up mainly of pink medium-grained hypersolvus granite which contains 40 % of quartz,
245 30 % of microcline, 20 % of perthitic orthoclase, biotite and green hornblende (Fig. 7a and b).
246 Accessory minerals correspond mainly to magnetite, zircon, apatite and euhedral sphene.
247 Myrmekite is generally abundant at the contact between plagioclase and K-feldspar. Many
248 metre to hectometre-scale enclaves and raft of country rocks have been observed in this
249 granite (Fig. 7c). We also found in the Sherubrub pluton some bodies of grey and medium-
250 grained granite (Fig. 3). The pluton is associated in its periphery with a spectacular swarm of
251 pegmatites which are intrusive in paragneisses and gabbros (Fig. 7d). The Sherubrub pluton
252 shows sharp and subvertical contacts with it country rocks. Microstructural study indicates
253 that the Sherubrub granites present a progressive evolution from the core of the pluton where
254 sub-solidus deformation occurred (Fig. 7a) to the contact where high-temperature solid state
255 deformation occurred (protomylonites) and where we have measured sub-vertical E-W
256 foliation planes (Fig. 7b)

257 The Mont-Haggier pluton consists of two major facies covering *ca.* 250 km^2. The
258 Northern-Haggier biotite granite covers *ca.* 60 km^2 around Hadibo. It corresponds to a light
259 grey and medium-grained granite which contains 40 % of quartz, 20 to 30 % of zoned
260 plagioclase, 20 to 30 % of myrmekitic alkali felspar and 10 % of biotite and green hornblende
261 (Fig. 7e). Accessory minerals correspond to apatite, zircon, magnetite and other opaque
262 minerals. Granite is associated with many mafic enclaves. Locally granites are more
263 leucocratic and present rare muscovite. Microstructural study indicate that the Northern-
264 Haggier biotite granite has suffered a very weak solid-state deformation marked by internal
265 deformation and reorientation of quartz grains (Fig. 7e).The Haggier pink granite covers *ca.*
266 200 km^2 in the centre of the Haggier basement high and can be studied on a natural vertical
267 cross-section of 1,500 metres. This granite is pinkish to reddish (Fig. 7f and 8a), and generally
268 coarse-grained. Quartz (~ 30%) and perthitic alkali feldspar (~ 60%) with subordinate albite
269 grains are the main components. We observed also rare arfvedsonite (Fig. 8b), zircon,
270 monazite and magnetite. The Haggier pink granite is generally devoid of internal deformation,
271 even though few thin-sections display quartz grains deformed under high-temperature

conditions (chessboard texture, Fig. 8c). The eastern contact of the Haggier pink granite with the layered gabbros, which correspond to the bottom of the pluton, is diffuse, characterized by spectacular magmatic "breccias" (Fig. 8a), and dip moderately at map scale. Magmatic "breccias" are characterized by stronly angular and numerous enclaves of gabbro in granites showing that the gabbros were crystallized at the time of granite intrusion. The southern and western limits of the pluton show sharps and subvertical contacts with the Southern Haggier volcanic series that may be followed for several kilometres. Study of the various contacts suggest that the pluton were developped mainly in the Southern Haggier volcanic series at the top of the Haggier layered gabbros. Finally, we observed from top to bottom of the batholith, an evolution of the texture of the granites, coarse-grained in the major part of the outcrop, and fine-grained in the western part of the Mont-Haggier area close to the contact with the Cenozoic and Mezosoic series.

The Haggier dike swarm

A spectacular amount of dikes has been observed in the Mont-Haggier area. We have not performed an exhaustive mapping of these dikes. Only the largest ones have been represented on the petrographic map (Fig. 2). We distinguish three generations: (i) dikes of microgranites, (ii) basaltic and andesitic dikes, (iii) dacitic and rhyolitic dikes.

Dikes of pink to red and fine grained granite are clearly associated with the pink Haggier granite intrusion and are ubiquous to the west and to the north of this intrusion. Metre to hectometre-scale microgranitic dikes present a microgranular porphyric texture with the same mineral association as the Haggier pink granite. While measurements of dikes of pinkish microgranites show some disparities (Fig. 9a), a major family can be easily identified, oriented on average around N33°E and subvertical.

Numerous volcanic dikes are intrusive in all the formations of the Mont-Haggier area. The pink Haggier granite is devoid of mafic dikes and is only cut by numerous rhyolitic dikes. Mafic dikes are homogeneously oriented (mean at N59°E, Fig. 9b) and correspond dominantly to basaltic dikes, rich in green hornblende and plagioclase, with a doleritic texture (Fig. 8d and e). Rhyolitic dikes (Fig. 8f) are homogeneously oriented (mean at N41°E, Fig. 9c) and display a microlithic-porphyric texture with orthoclase megacrysts.

Major and trace elements

Several mafic and felsic rocks from Mont-Haggier, Sherubrub and Qalansya basement were sampled for whole-rock analysis (Table 1). Mafic rocks were picked up at Mont Haggier and Qalansya areas whereas analysed felsic rocks were selected from Mont Haggier and Sherubrub samples.

Mafic rocks

According to geochemical data, mafic rocks from Socotra Island suffered different degrees of alteration. The Haggier layered gabbros are the least altered rocks with Loss on Ignition (LOI) below 1.6 wt.%. Most Basaltic dikes belonging to the Haggier dike swarm (SP10 and SP18), basaltic lava (S20) and tuff (SP16B) from the Southern Haggier volcanic series are significantly altered with LOI up to 3.8 wt.% (Table 1). Diorites (CS14A and CS18A) from the mafic to intermediate plutonic sheets of Qalansya are almost fresh rocks (LOI = 2.01 wt.% and 0.98 wt.%). The yellowish basalt croping out in the Northern part of the Mont-Haggier area is highly altered (SP15A: LOI = 5.99 wt.%).

Major elements composition of volcanic and subvolcanic rocks from Mont-Haggier are in good agreement with those of basalts, basaltic andesites and andesites (Table 1), even though MgO and CaO concentrations are significantly low most likely due to strong differentiation process. According to the SiO_2 vs K_2O diagram (Fig. 10), three volcanic and subvolcanic rocks (SP10, SP16bB and SP18A) are calc-alkaline in composition whereas the yellowish basalt SP15A belong to the high-K calc-alkaline to shoshonitic field. However, due to high LOI values, such discrimination should be used with caution. For example, sample S20 falls in the arc tholeiites series field most likely due to Large-Ion Lithophile Element (LILE) leaching during alteration process. Diorites of Qalantsya are calc-alkaline (CS18A) or high-K calc-alkaline (CS14A) in composition. Mafic to intermediate rocks from Mont-Haggier show a wide range of Al_2O_3 (13.52-26.32 wt.%), Fe_2O_3 (2.71-13.99 wt.%), CaO (5.20-14.78 wt.%), MgO (2.43-7.55 wt.%), TiO_2 (0.18-2.56 wt.%) and Mg# (17-56) reflecting difference between gabbro cumulates and non-cumulative rocks. Mafic to intermediate rocks from Qalansya display almost homogeneous geochemical composition except for SiO_2 (49.38 vs. 54.55 wt.%) and Fe_2O_3 (8.48 vs. 11.15 wt.%). According to trace elements data, two different signatures can be distinguished from non-cumulative rocks (Fig. 11a and Fig. 11c; Table 1). The first signature recorded in the basalt SP15A and in the diorites of Qalansya, is

characterized by low Nb and Ta negative anomalies (La_N/Nb_N = 3-4) indicative of suprasubduction setting and by low LILE and LREE enrichment (e.g. Ce/Yb < 15) underlined by a relatively flat multi-element patterns in Figure 9a. The second signature, which is recorded in the volcanic and subvolcanic rocks of Mont-Haggier area shows a large negative Nb and Ta anomaly (La_N/Nb_N > 7) and shows significant enrichment in LILE and LREE (e.g. Ce/Yb >> 15) characteristic of volcanic arc basalts. In Figure 11d, the first group belongs to the arc calc-alkaline basalts field and the second group plots in the transitional arc basalts field and is close to arc tholeiite basalts (i.e. immature arc basalt) and back-arc basalt field. Gabbro cumulates (Fig. 11a and Fig. 11b) are geochemically related to the second group as underlined by chondrite-normalized rare earth elements diagram (Fig. 11b) which emphasizes an evolution by fractional crystallization process. As a consequence, major and trace elements composition of mafic to intermediate rocks highlights existence of two distinct geochemical compositions in Socotra basement (Figure 11a, 11c and 11d; Table 1): (i) a signature diagnostic of a depleted-arc or back-arc basin setting, and (ii) a signature characteristic of enriched-arc setting.

Felsic rocks

Felsic rocks from the Haggier dike swarm, and the Haggier and Sherubrub plutons display a moderate range of chemical composition (Table 1) with high SiO_2 content (71.67-78.50 wt.%), low to moderate contents of Al_2O_3 (11.22-14.34 wt.%) and Fe_2O_3 (0.91-3.47 wt.%), low levels of MgO and TiO_2 (< 0.53 wt.% and < 0.37 wt.% respectively), and moderate to high alkalies concentrations (Na_2O : 2.95-5.33 wt.%; K_2O : 3.02-5.81 wt.%). In Figure 12a, felsic rocks are distributed between peraluminous, metaluminous and peralkaline fields although most analyses are characterized by a metaluminous composition. Trace elements data underlines wide variations in MREE, HREE, Zr and Hf, whereas LILE (except Ba) and LREE composition exhibit a relative narrow range of composition (Fig. 12b) resulting in relatively low LREE/HREE ratios (e.g. La_N/Yb_N <6.7). Nb and Ta may be highly variable but always display negative anomalies on silicate Earth-normalized multi-elements diagram (Fig. 12b). Based on the plot of 10000*Ga/Al vs. Zr + Nb + Y + Ce, felsic rocks from both Mont Haggier and Sherubrub areas fall in the field of A-type granite except for two samples which belong to the field of I-M-S-type granites (Fig. 12c). However, in similar plots (i.e 10000*Ga/Al vs. Nb; 10000*Ga/Al vs. Y; 10000*Ga/Al vs. Ce; not shown) analyses show a complex and transitional signature as they fall between fractionated I-type granite and

A-type granite fields. On a discrimination diagram (Fig. 12d), felsic rocks plot both within the volcanic arc/syn-collision and oceanic ridge granites fields, except for one sample located in the within plate granite field. Thus, geochemistry of felsic rocks from Socotra is not entirely consistent with anorogenic (ORG and WPG) and orogenic (VAG) signature and their emplacement in Cryogenian in a back-arc setting cannot be ruled out.

U/Pb data

Three samples were collected for zircon U-Pb dating. HAEU-1 and HAEU-2 (localization in fig.2) were collected in the Mont-Haggier area. HAEU-1 is representative of the Haggier pink granite. HAEU-2 corresponds to an enclave of gabbro in the Haggier pink granite, showing the same petrographic characteristics of the Haggier layered gabbros. Other sample (SHEU-1, localization in fig.3) collected in the Sherubrub basement high, is representative of the pinkish granite of the Sherubrub pluton.

Zircon grains from each sample were selected by hand-picking from 50-300 μm fractions and mounted in epoxy resin together with fragments of the 91,500 standard zircon, dated at 1062.4 ± 0.4 Ma [Ontario, Canada; Wiedenbeck et al., 1995]. Mounts were then polished and gold coated. U-Pb isotopic compositions were determined in situ using the CRPG-CNRS Cameca IMS-1270 ion microprobe (Nancy, France). Further information on instrumental conditions and data reduction procedures is given in Deloule et al. (2002). Concordia diagrams and discordia lines were constructed using the Isoplot program (Ludwig, 2003). In the forthcoming paragraphs, we use $^{206}Pb/^{238}U$ ages for concordant data, rather than $^{207}Pb/^{235}U$ ages, which are more sensitive to common lead contribution (the ^{207}Pb ion signal is about ten times lower than the ^{206}Pb ion signal). Discordant data were used on the concordia diagrams to calculate possible discordia lines.

Eleven anhedral to squat zircon grains were analysed for sample HAEU-1 and for each crystal core and rim were analysed (Table 2). Analyses show very small common lead contribution but significant Pb losses. One zircon grain provides a concordant $^{206}Pb/^{238}U$ age at 858 ± 11 Ma and is interpreted as an inherited core. The remaining ten analyses are subconcordant or discordant. Regression curve calculated from these zircon grains gives a discordia line (Fig. 13a) with an upper intercept at 816 ± 12 Ma (MSWD = 0.49).

Eleven zircon grains were analysed for sample HAEU-2 and for each crystal core and rim were analysed (Table 2). Based on morphology, two types of zircons can be identified: (i)

euhedral and acicular crystals and (ii) anhedral to subhedral and squat crystals. Data show very small amount of common lead (Pbc < 1%) but some exhibit slight Pb or U losses. One zircon grain gives concordant $^{206}Pb/^{238}U$ age at 856 ± 12 Ma and most likely corresponds to an inherited core. Seven of the remaining eleven analyses are scattered along discordia line (Fig. 13b) defining an upper intercept at 825 ± 18 Ma (MSWD = 0.49). Mean $^{206}Pb/^{238}U$ age of 821 ± 16 Ma (MSWD = 0.53) was calculated from four subconcordant analyses. Since gabbro enclaves are intruded by some granitic veins, we assume the presence of two population of zircon: (i) one associated with the gabbro enclaves and (ii) and the other crystallized from the granitic intrusions and veins. However, taking into account the low zirconium concentrations of gabbros and the very low abundance of zircon observed in thin sections, we assume that most zircon crystals separated from HAEU-2 belong to granitic intrusions and veins. Even if some zircon grains from gabbros enclaves have been analysed, homogenous distribution of data observed in Fig.13b indicates a relative contemporaneity (within 206Pb/238U age errors) of mafic and felsic magmatism. Whatever, calculated U-Pb age is identical within errors to age obtained for the sample HAEU-1 and is interpreted as the age of emplacement of the Haggier pink granite.

In the Sherubrub granite (sample SHEU-1), zircon grains are euhedral, prismatic and acicular. One zircon analysis displays slight loss of uranium linked to a reopening of the U-Pb system. The remaining seven analyses are subconcordant to discordant. Regression of these zircon analyses provides a discordia line (Fig. 13c) with an upper intercepts at 812 ± 27 Ma (MSWD = 1.8). This age is in good accordance with ages acquired from the only concordant analysis on a Tera-Wasserburg diagram (not shown) i.e. 809 ± 13 Ma ($^{206}Pb/^{238}U$ age) and 815 ± 11 Ma ($^{207}Pb/^{235}U$ age).

Discussion

The high-temperature metamorphic stage of the Socotra basement

The oldest rocks of Socotra correspond mainly to an association of paragneisses and quartzites forming the metamorphic basement. Protolith of these rocks probably correspond to an alternation of metapelite, sandstone and argillaceous sandstone which could correspond to delta or continental shelf deposits. These rocks were metamorphosed and deformed under amphibolite facies conditions reaching partial melting, and were intruded coevally by gabbros

441 and granites which now form interfoliated lenses or boudins of ortho-amphibolites and
442 orthogneisses. These metamorphic rocks show many lithological similarities with the Juffa
443 group in Oman (Mercolli et al., 2006) which corresponds to an alternation of paragneisses,
444 micaschists and ortho-amphibolites, and the Banded Gneiss Complex which corresponds to an
445 association of augengneisses and biotite-hornblende gneisses. Steep foliation planes and
446 contacts between the various units of the metamorphic basement of Socotra suggest that
447 metamorphism and deformation occurred in a compressive or in a transpressive regime. Our
448 U-Pb data in granites show scarcity of inherited cores represented by two zircons with U-Pb
449 ages at *ca.* 860 Ma. These measurements suggest that the orthogneisses, migmatites and
450 orthoamphibolites of Socotra are younger than 860 Ma. This is consistent with both datation
451 of emplacement of the protolith of the orthogneisses of the Banded Gneiss Complex and
452 datation of the metamorphic event in the Juffa Group and the Banded Gneiss Complex around
453 815 Ma obtained by Mercolli et al. (2006). However we have no elements to precise the age
454 of the protoliths of the paragneisses and quartzites that could be of Mesoproterozoic age as
455 the Juffa Group in Mirbat (Mercolli et al., 2006).
456
457 *Mafic intrusions on the Cryogenian active margin of Socotra*
458
459 Metamorphic rocks of the Socotra basement have been intruded by voluminous mafic
460 and felsic magmatic bodies. Field relationships show that felsic intrusions occur generally
461 later than the mafic to intermediate one. Mafic to intermediate bodies of Socotra show some
462 evidences of metamorphic overprint in amphibolite facies conditions. However these rocks
463 have not suffered the strong solid-state deformation recorded by the metamorphic basement
464 and are devoid of evidence of partial melting. Emplacement of mafic to intermediate
465 intrusions is thus late-kinematic and post-date metamorphic peak. The mafic to intermediate
466 plutonic sheets have been affected by an incipient solid-state deformation and show discrete
467 steeply dipping foliation planes parallel to those of the metamorphic basement. These sheets
468 correspond probably to the first mafic intrusions.
469 Mafic rocks were characterized by two distinct signatures. A signature diagnostic of a
470 depleted-arc or back arc basin ($Ce/Yb > 15$; $La_N/Nb_N > 7$) is recorded in the mafic rocks
471 belonging to the Mont-Haggier area as the Haggier layered gabbros, the basaltic lavas of the
472 Southern Haggier volcanic series and the mafic dikes of the Haggier dike swarm. The Haggier
473 mafic system allows thus the observation of a well-preserved upper part of a juvenile arc or a
474 back-arc basin (Fig. 14), with a magmatic chamber characterized by crystallization of

cumulates, volcanic effusions in surface and formation of a dike swarm which allowed the magmas to be transfered from the magmatic chamber to the surface. The second signature of mafic to intermediate rocks is characteristic of enriched-arc setting (Ce/Yb > 15 ; La/Nb > 6.5) and is evidenced in the yellowish basalt SP15A and in the diorites of the mafic to intermediate plutonic sheets of Qalansya. The low contents of HREE compared to the orthers REE of the sample SP15A (e.g. La/Yb > 80) could indicate the presence of garnet in the source of this basalt and thus a genesis at high depth.

Geochemical compositions of the mafic rocks of Socotra indicate clearly a suprasubduction context during the middle Neoproterozoic times (Cryogenian). The first mafic rocks were emplaced in a context of an enriched-arc setting forming probably in an Andean-type arc. By contrast the last emplaced mafic rocks of Socotra are characteristic of a depleted-arc context which could correspond to the formation of either (i) an intra-oceanic island-arc, (ii) or an island-arc above a thinned continental crust, or (iii) a back-arc basin. By considering that the basement of Socotra is affected by an important HT-LP metamorphism prior and coevally with the formation of the depleted-arc, we suggest that emplacement of mafic rocks presenting a depleted-arc signature occurred during the opening of a back-arc basin. This hypothesis provides also an explanation to understanding the contrasted structural features between the gabbros cumulates characterized by moderately dipping magmatic layering that can be formed during local extensional regime, and steeply dipping calc-alkaline sheets that probably intruded the metamorphic basement during compressive regime. Homogeneous orientation of basaltic dikes around N60°E indicates that the back-arc basin (or juvenile arc) of Socotra is probably aligned along the same direction during Cryogenian times (Fig. 14).

The sheets of mafic to intermediate rocks of Socotra correspond probably to an equivalent of the Mahall Complex of Mirbat (Mercolli et al., 2006), which intruded the Juffa group around 800 Ma and and corresponds to original dioritic and tonalitic plutons that have been deformed and recrystallised under amphibolite facies conditions. The juvenile arc system of Socotra including cumulates, basaltic dikes and tholeitic lavas could correspond to an equivalent of the Tonalite Group in Mirbat which have been dated between 790 and 780 Ma and have never suffered solid-state deformation (Mercolli et al., 2006). The Tonalite Group comprises two small bodies of hornblende bearing layered olivine gabbroic intrusions which are petrographically similar to the Haggier layered gabbro body, and two kilometre-scale tonalite to granodiorite layered plutons, the Hadbin and Fusht Complex. Al-Kathiri (1998) suggested that the layered gabbros of Mirbat represent the parental magmas from

509 which the dioritic-tonalitic rocks of the Fusht and Hadbin complex evolved by hornblende
510 dominated fractionation. Although in Mirbat volcanic rocks that could correspond to the
511 Southern Haggier volcanic Series were never found, volcanic clasts are very abundant in the
512 sediments of the Ediacaran clastic Mirbat formation (Mercolli et al., 2006). This suggest that
513 the volcanic series representing the upper crustal level during Cryogenian times were largely
514 eroded during Ediacaran in the Mirbat basement as in the western part of the Socotra Island.
515
516 *The Cryogenian High-K calc-alkaline intrusions of Socotra*
517
518 The Sherubrub pluton intrusive in the Sherubrub gabbro and in the metamorphic
519 basement shows systematic vertical and sharp contacts with it country rocks. While
520 emplacement of this pluton is clearly post-metamorphic peak, strong high to middle
521 temperature deformation at the contact with it country-rocks associated with a sub-vertical
522 solid-state foliation suggests a syn-collisional emplacement in compressive regime. The
523 Haggier pink granite was clearly intrusive at the top of the Haggier layered gabbros (Fig. 14)
524 when these gabbros were crystallized as shown by the presence of magmatic breccia. These
525 granites have suffered a very weak deformation and emplaced at the top of the upper crustal
526 domain as shown by their textural evolution from the top to the base of the pluton. Finally the
527 Northern Haggier biotite granite crops out in a low-relief zone and we were not able to study
528 relationship between this granite and its country-rocks. This granite is intruded by some
529 basaltic dikes (Fig. 14) presenting the same geochemical affinity of the Haggier layered
530 gabbros. We can thus suggest that emplacement of the Northern Haggier biotite granite is
531 coeval with the final stage of emplacement of mafic rocks. Whereas U-Pb datation on the
532 Haggier pink granite and the Sherubrub granites present important uncertainties, ages are very
533 close and suggest in accordance with geochemical data that felsic plutons of Socotra were
534 emplaced during the same magmatic activity which occurred between 840 and 780 Ma.
535 Granites and felsic dikes present geochemical characteristics which underline their
536 transitional character although with a certain affinity with A-type granites. Also the
537 geochemical diagrams do not associate them with a distinct geodynamic setting, however
538 field relationships suggest that their emplacement occurred by the end of the Cryogenian
539 active margin formation. Orientations of microgranitic and rhyolitic dikes associated with the
540 Haggier pink granite are very close to the orientation of the basaltic dikes, and are thus
541 consistent with this hypothesis (Fig. 14). Moreover structural data in the Sherubrub pluton
542 suggest that their emplacement occured during compressive regime. In this way, emplacement

543 of these granites could correspond to the final stage of the orogenic system evolution during
544 the closure of a back-arc system in an Andean type margin.
545 The Mirbat block presents a later calc-alkaline acidic magmatism event characterized by
546 some hectometric-scale bodies of granite and by the developement of a pegmatitic dike
547 swarm (Mercolli et al., 2006). Mirbat is thus less or not affected by the voluminous high-
548 potassic acidic magmatic event that we have observed in Socotra. Subsequently to these
549 Cryogenian events, the various units of Mirbat recorded fast exhumation (Mercolli et al.,
550 2006). The mirbat basement rocks are overlain by clastic sediments of the Mirbat formation
551 which is probably Ediacaran in age (Mercolli et al., 2006). The Hadibo series (Beydoun and
552 Bichan, 1970) are composed mainly by sandstones. These clastic series are restricted to the
553 footwall of the main transfer fault of Socotra (Fig. 2) and overlain the Cryogenian basement.
554 These series recorded probably as the Mirbat formation, Ediacaran denudation of the
555 Cryogenian basement of Oman.
556
557 *The Socotra and Mirbat basements in the case of the East-African-Antartic-Orogen*
558
559 Our study of the Neoproterozoic Socotra basement underlines formation of a juvenile
560 arc system and/or back-arc basin with some evidences of evolution from an Andean-type arc.
561 Formation of this system is late compared to a stage of HT-LP metamorphism that was
562 recorded in the older metasedimentary rocks of Socotra. Although we have insufficient
563 geochronological data to constrain the ages of the earliest events recorded in the Socotra
564 basement, we can claim on the basis of our data on Socotra and by analogy with the Mirbat
565 block in Oman: (i) that the basement of Socotra is affected by a high temperature
566 metamorphic stage whose minimum age is 815 Ma; (ii) that the metamorphic basement is first
567 intruded by mafic to intermediate rocks related to an Andean type arc and secondly by mafic
568 rocks related to a juvenile arc/or back-arc basin; and (iii) that the arc system is intruded by
569 large acidic plutons with a transitional affinity, these plutons being characterized by a
570 minimum age at 780 Ma.
571 The comparison of these characteristics with those of the various domains of the EAAO
572 provides more information. Between 700 and 600 Ma, the ANS suffered a low to medium
573 grade metamorphism linked to terrane accretion. This metamorphic stage is younger than the
574 juvenile arc formation which occurred mainly between 800 and 700 Ma (e.g. Nehlig et al.,
575 2002; Johnson and Woldehaimot, 2003). The Mozambic belt in the central and southern part
576 of the EAAO is characterized by coeval deformation and high-temperature metamorphism,

577 marked by formation of granulites, between *ca.* 600 and 540 Ma (Jacobs and Thomas, 2004).
578 The terranes of the continental Yemen show the transition between the ANS and the high-
579 grade rocks of the EAAO. The Al-Mafid and Abas gneiss terranes (Fig. 1b) recorded a major
580 ca. 760 Ma metamorphism and deformational event linked to terranes accretion and marked
581 by Pb loss in zircons in Archean gneisses and by zircon crystallization ages of granitic
582 gneisses (Whitehouse et al., 1998). Moreover $^{40}Ar/^{39}Ar$ ages obtained from intrusive rocks at
583 the boundary between Al-Mafhid and Abas gneiss terranes provide a lower limit of 615 Ma
584 upon terrane assembly (Whitehouse et al., 1998). The basements of Socotra and Mirbat
585 present a high-grade metamorphic stage earliest than that recorded in the pan-african EAAO.
586 The magmatic rocks of the ANS present generally a typical volcanic-arc signature while the
587 magmatism of Socotra shows a complex evolution in a short time span with very peculiar
588 geochemical signatures, that suggest an evolution from an Andean-type arc to a juvenile
589 arc/back-arc basin with later emplacement of large high-potassic plutons. Finally, structural
590 studies indicate that the major foliation planes are homogeneously oriented between N70°E
591 and N80°E in Socotra and Mirbat (Mercolli et al., 2006), whereas the main directions
592 underlined in the ANS are NS to NW-SE (Johnson and Woldehaimot, 2003, references
593 therein).

594 These comparisons suggest that the basement of Mirbat and Socotra were formed in a
595 different geodynamic setting from those of the ANS and the high-grade Mozambic belt of the
596 EAAO. Though there is a lack of paleomagnetic data to have a detailled paleogeographic
597 reconstruction of this period, we consider following Li et al. (2008) that the microcontinental
598 blocks of Afif-Abbas and Al-Mahfid were placed between India and Sahara in Cryogenian
599 times. Many evidences highlight that a Cryogenian active Andean-type margin was developed
600 on the western part of the Greater India block (Li et al., 2008). This active margin has been
601 identified by using integrated geochronological, geochemical and paleomagnetic analysis in
602 Seychelles Islands (Torsvik et al., 2001a; Tücker et al., 2001; Ashwal et al., 2002), in
603 northwestern India with the Malani Igneous Suite (Torsvik et al., 2001b) and in northeastern
604 Madagascar (Tucker et al., 1999a and b). In the Seychelles Islands this active margin is
605 marked by emplacement of two groups of granites dated around 750 Ma: the Mahé group
606 which corresponds to greyish granites and the Praslin group which corresponds to redish to
607 pinkish granites (Ashwal et al., 2002). These two granites present many petrographic and
608 geochemical similarities with both the greyish and pinkish granites of Socotra, which
609 indicates that the Neoproterozoic rocks of Socotra could also form on the Cryogenian

Andean-type margin of the Indian block. This hypothesis would need additional structural, isotopic and more geochronological data to be tested.

Conclusion

The basement of the Socotra Island presents an early high-temperature metamorphism event associated with a strong deformation and then a voluminous mafic and felsic emplacement event. U-Pb data indicate that these successive events occurred during a relative short time span, between 860 and 780 Ma at maximum. Mafic magmatism shows the evolution from an Andean type arc to a juvenile arc/or back-arc basin. Felsic magmatism is characterized by emplacement of voluminous highly potassic calc-alkaline granites forming large plutons and which occurred probably at the final stage of arc history. These granites are not anorogenic as it has been previously published by analogy to the peralkaline granites of the ANS which were emplaced at *ca.* 600 Ma.

These features cannot be easily reconciled with those of the Arabian-Nubian Shield to the west of Socotra and with the Mozambique Belt to the south. We propose that the Socotra basement was developed on an active margin located near the Indian block in Cryogenian times.

Acknowledgements

We thank Ph. Olivier and L. Siebenaller for constructive discussions.

We also thank P. Barbey and I. Mercolli for their valuable remarks which helped us to improve a first version of this article.

Bibliography

Ashwal LD, Demaiffe D, Torsvik TH (2002) Petrogenesis of Neoproterozoic granitoids and related rocks from the Seychelles: the case for an Andean-type arc origin. J. Petrol. 43: 45–83.

642 Avigad D, Gvirtzman Z (2009) Late Neoproterozoic rise and fall of the northern Arabian–
643 Nubian shield: The role of lithospheric mantle delamination and subsequent thermal
644 subsidence. Tectonophysics 477: 217–228.

645 Bingen B, Jacobs J, Viola G, Henderson IHC, Skår Ø, Boyd R, Thomas RJ, Solli A, Key RM,
646 Daudi EXF (2009) Geochronology of the Precambrian crust in the Mozambique belt in
647 NE Mozambique, and implications for Gondwana assembly. Precambrian Res. 170: 231–
648 255.

649 Beydoun ZR, Bichan HR (1970). The geology of Socotra Island, Gulf of Aden. Quaterly J.
650 Soc. Lond. 25: 413–446.

651 Blasband B, Brooijmans B, Dirks P, Vissers W, White S (1997) A Pan-African core complex
652 in the Sinai, Egypt. Geol. Mijnb. 76: 247–266.

653 Blasband B, White S, Brooijmans B, De Boorder H, Visser W (2000) Late Proterozoic
654 extensional collapse in the Arabian–Nubian Shield. J. Geol. Soc. Lond. 157: 615–628.

655 Cabanis B, Lecolle M (1989) Le diagramme La/10-Y/15-Nb/8; un outil pour la discrimination
656 des series volcaniques et la mise en evidence des processus de melange et/ou de
657 contamination crustale. CRAS, Paris 309: 2023–2029.

658 Collins AS, Pisarevsky SA (2005) Amalgamating eastern Gondwana: the evolution of the
659 Circum-Indian Orogens. Earth-Sci. Rev. 71: 229–270.

660 Collins AS (2006) Madagascar and the amalgamation of Central Madagascar. Gondwana Res.
661 (GR Focus) 9: 3–16.

662 d'Acremont E, Leroy S, Maia M, Patriat P, Beslier M-O, Bellahsen N, Fournier M, Gente P
663 (2006) Structure and evolution of the eastern Gulf of Aden: insights from magnetic and
664 gravity data (Encens–Sheba/MD117 cruise). Geophys. J. Int. 165: 786–803.

665 Deloule E, Alexandrov P, Cheilletz A, Laumonier B, Barbey P (2002) In-situ U-Pb zircon
666 ages for early Ordovician magmatism in the eastern Pyrenees, France: the Canigou
667 orthogneisses. Int. J. Earth Sci. 91: 398–405.

668 Gass G, Ries AC, Shackleton RM, Smewing JD (1990) Tectonics, geochronology and
669 geochemistry of the Precambrian rocks of Oman. In: Robertson AHF, Searle MP, Ries AC
670 (eds.) The Geology and Tectonics of the Oman Region. Spec. Pub. Geol. Soc. Lond. 49:
671 585–599.

672 Greiling R O, Abdeen MM, Dardir AA, El Akhal H, El Ramly MF, Kmal El Din GM, Osman
673 AF, Rahwan AA, Rice AA, Sadek MF (1994) A structural synthesis of the Proterozoic
674 Arabian-Nubian shield in Egypt. Geologische Rundshau 83: 484-501.

675 Johnson PR, Woldehaimanot B (2003) Development of the Arabian-Nubian shield:
676 perspectives on accretion and deformation in the northern East African Orogen and the
677 assembly of Gondwana. In: Yoshida M, Windley BF, Dasgupta S (eds) Proterozoic East
678 Gondwana: Supercontinent Assembly and Breakup. Spec. Pub. Geol. Soc. Lond. 206:
679 289–325.

680 Jacobs J, Fanning CM, Henjes-Kunst F, Olesch M, Paech HJ (1998) Continuation of the
681 Mozambique Belt into East Antarctica: Grenville-age metamorphism and polyphase Pan-
682 African high-grade events in central Dronning Maud Land. J. Geol. 106: 385–406.

683 Jacobs J, Thomas RJ (2004) Himalayan-type indenter-escape tectonics model for the southern
684 part of the late Neoproterozoic-early Paleozoic East African-Antarctic orogen. Geology
685 32: 721–724.

686 Jacobs J, Thomas RJ (2010) Himalayan-type indenter-escape tectonics model for the southern
687 part of the late Neoproterozoic–early Paleozoic East African–Antarctic orogen. Geol. Soc.
688 Am. 32: 721–724.

689 Kröner A, Willner AP, Hegner E, Jaeckel P, Nemchin A (2001) Single zircon ages, PT
690 evolution and Nd isotopic systematics of high-grade gneisses in southern Malawi and their
691 bearing on the evolution of the Mozambique belt in southeastern Africa. Precambrian Res.
692 109, 257–291.

693 LeBas MJ, LeMaitre RW, Streckeisen A, Zanettin B (1986) A chemical classification of
694 volcanic rocks based on the total alkali silica diagram. J. Pet. 27:745–750.

695 Leroy S, Gente P, Fournier M, d'Acremont E, Patriat P, Beslier M-O, Bellahsen N, Maia M,
696 Blais A, Perrot J, Al-Kathiri A, Merkouriev S, Fleury JM, Ruellan PY, Lepvrier C,
697 Huchon P (2004) From rifting to spreading in the eastern Gulf of Aden: a geophysical
698 survey of a young oceanic basin from margin to margin. Terra Nova 16: 185–192.

699 Leroy S, Lucazeau F, d'Acremont E, Watremez L, Autin J, Rouzo S, Bellahsen N, Tiberi C,
700 Ebinger C, Beslier M-O, Perrot J, Razin P, Rolandone F, Sloan H, Stuart G, Al-Lazki A,
701 Al-Toubi K, Bache F, Bonneville A, Goutorbe B, Huchon P, Unternehr P, Khanbari K
702 (2010a) Contrasted styles of rifting in the eastern Gulf of Aden: a combined wide-angle

703 MCS and Heat flow survey. Geochemistry, Geophysics, Geosystems 11 (Q07004):1–14.
704 doi:doi:10.1029/2009GC002963.

705 Leroy S, d'Acremont E, Tiberi C, Basuyau C, Autin J, Lucazeau F, Sloan H (2010b) Recent
706 off-axis volcanism in the eastern Gulf of Aden: implications for plume-ridge interaction.
707 Earth Planet Sci. Lett. 293 (1-2):140–153. doi:10.1016/j.epsl.2010.02.036.

708 Leroy S, Razin P, Autin J, Bache F, d'Acremont E, Watremez L, Robinet J, Baurion C,
709 Denèle Y, Bellahsen N, Lucazeau F, Rolandone F, Rouzo S, Serra Kiel J, Robin C,
710 Guillocheau F, Tiberi C, Basuyau C, Beslier M-O, Ebinger C, Stuart G, Sloan H, Ahmed
711 A, Khanbari K, Al-Ganad I, de Clarens P, Unternehr P, Al-Toubi K, Al-Lazki A
712 (submitted in this volume) Rifting to spreading in the Gulf of Aden.

713 Li ZX, Powell CM (2001) An outline of the Palaeogeographic evolution of the Australasian
714 region since the beginning of the Neoproterozoic. Earth-Sci. Rev. 53: 237–277.

715 Li ZX, Bogdanova SV, Collins AS, Davidson A, De Waele B, Ernst RE, Fitzsimons ICW,
716 Fuck RA, Gladkochub DP, Jacobs J, Karlstrom KE, Lu S, Natapov LM, Pease V,
717 Pisarevsky SA, Thrane K, Vernikovsky V (2008) Assembly, configuration, and break-up
718 history of Rodinia: A synthesis. Precambrian Res. 160: 179-210.

719 Ludwig KR (2001) User manual for Isoplot/Ex rev. 2.49. A geochronological toolkit for
720 Microsoft Excel. Berkeley Geochronology Center, Special Publication 1: 56 pp.

721 McDonough WF, Sun S-S (1995) The composition of the Earth. Chem. Geol. 120: 223–253.

722 Maniar PD, Piccoli, PM (1989) Tectonic discrimination of granitoids. Geol. Soc. Am. Bull.
723 101:635–643.

724 Meert JG (2003) A synopsis of events related to the assembly of eastern Gondwana.
725 Tectonophysics 362: 1–40.

726 Mehnert K R (1968) Migmatites and the Origin of Granitic Rocks. Elsevier Sci., New York:
727 393 pp.

728 Mercolli I, Briner AP, Frei R, Schonberg R, Nägler, TF, Kramers J, Peters T (2006)
729 Lithostratigraphy and geochronology of the Neoproterozoic crystalline basement of
730 Salalah, Dhofar, Sultanate of Oman. Precambrian Res. 145: 182–206.

731 Muhongo S, Lenoir J-L (1994) Pan-African granulite-facies metamorphism in the
732 Mozambique belt of Tanzania: U–Pb zircon geochronology. J. Geol. Soc. Lond. 151, 343–
733 347.

734 Nehlig E, Genna A, Asfirane, E (2002) A review of the Pan-African evolution of the Arabian
735 Shield. GeoArabia 7: 103–124.

736 Pearce JA, Harris BW, Tindle AG (1984) Trace element discrimination diagrams for the
737 tectonic interpretation of granitic rocks. J. Petrol. 25: 956–983.

738 Razin P, Leroy S, Robin C, Robinet J, Serra Kiel J, Bellahsen N, Grelaud C (2010) Dispositifs
739 tecto-sédimentaires syn-rift et post-rift Oligo-Miocènes sur la marge sud du Golfe d'Aden.
740 Paper presented at the RST, Bordeaux, octobre 2010.

741 Saint Blanquat (de) M, Horsman E, Habert G, Morgan S, Vanderhaeghe O, Law R, Tikoff B
742 (2010) Multiscale magmatic cyclicity, duration of pluton construction, and the paradoxical
743 relationship between tectonism and plutonism in continental arcs. Tectonophysics:
744 doi:10.1016/j.tecto.2009.12.009.

745 Shackleton RM (1996) The final collision zone between East and West Gondwana: Where is
746 it? J. Afric. Earth Sci. 23: 271–287.

747 Stern RJ (1994) Arc Assembly and Continental Collision in the Neoproterozoic East-African
748 Orogen—implications for the consolidation of Gondwanaland. Ann. Rev. Earth Planet.
749 Sci. 22: 319–351.

750 Sun S-S, McDonough WF (1989) Chemical and isotopic systematics of ocean basalts:
751 implications for mantle composition and process. In: Saunders AD, Norry MJ (eds.)
752 Magmatism in the Ocean Basins. Spec. Pub. Geol. Soc. Lond. 42: 313–345.

753 Torsvik TH, Carter LM, Ashwal LD, Bhushan SK, Pandit MK, Jamtveit B (2001a) Rodinia
754 refined or obscured: palaeomagnetism of the Malani igneous suite (NW India).
755 Precambrian Res. 108: 319–333.

756 Torsvik TH, Ashwal LD, Tucker RD, Eide EA (2001b) Neoproterozoic geochronology and
757 palaeogeography of the Seychelles microcontinent: the India link. Precambrian Res. 110:
758 47–59.

759 Tucker RD, Ashwal LD, Hancke MJ, Hamilton MA, Le Grange M, Rambeloson, RA (1999a)
760 U-Pb geochronology and isotope geochemistry of the Archean and Proterozoic rocks of
761 north-central Madagascar. J. Geol. 107: 135–153.

762 Tucker RD, Ashwal LD, Torsvik TH (1999b) Neoproterozoic silicic magmatism in northern
763 Madagascar, Seychelles and NW India: clues to Neoproterozoic supercontinent formation
764 and dispersal. EOS Transactions, Am. Geophys. Union 80: 372–373.

765 Tucker RD, Ashwal LD, Torsvik TH (2001) U–Pb geochronology of Seychelles granitoids: a
766 Neoproterozoic continental arc fragment. Earth Planet. Sci. Lett. 187: 27–38.

767 Whalen JB, Currie KL, Chappell BW (1987) A-Type granites: Geochemical characteristics,
768 discrimination and petrogenesis. Contrib. Mineral. Petrol. 95:407–419.

769 Whitehouse MJ, Windley BF, Ba-bttat MAO., Fanning CM, Rex DC (1998) Crustal evolution
770 and terrane correlation in the eastern Arabian Shield, Yemen: geochronological
771 constraints. J. Geol. Soc. Lond. 155: 281–295.

772 Whitehouse MJ, Windley BF, Stoeser DB, Al-Khirbash S, Ba-Bttat MAO, Haider A (2001)
773 Precambrian basement character of Yemen and correlations with Saudi Arabia and
774 Somalia. Precambrian Res. 105: 357–369.

775 Whitney DL, Evans B (2010) Abbrevations for names of rock-forming minerals. Am.
776 Mineralogist 95: 185-187.

777

778

779 **Figure caption**

780

781 Fig. 1: a) Reconstitution of the late Neoproterozoic EAAO (modified from Jacobs and
782 Thomas, 2004). Abbreviations: EF = European fragments, M = Madagascar, S = hypothesis
783 for the paleoposition of the Socotra Island at the end of the Neoproterozoic. b) Geological
784 map of the Arabian-Nubian Schield (modified from Whitehouse et al., 1998, Nelhig et al.,
785 2002; Jonhson and Woldehaimot, 2003).

786

787 Fig. 2: Geological and topographic map of Socotra. Topographic contours have been realized
788 by using the SRTM data (2001). Oligo-Miocene structures are from Razin et al. (2010).

789

790 Fig. 3: Detailed geological map of the Sherubrub area.

791

792 Fig. 4: Field photographs, microphotographs (scale bar = 2 mm); a) Ortho-amphibolitic
793 boudins in white quartzites (Sherubrub area); b) Bt+Sil+Afs±And (see Whitney and Evans,

794 2010 for mineral abbreviations) paragenesis in migmatitic paragneiss (metatexite) at the
795 contact between leucosom and melanosom (plane polarized light); c) Gabbro metamorphised
796 in the amphibolite-facies (planar polarized light, Mont Haggier area); d) Pyroclastic basaltic
797 breccia; e) Basaltic tuff with breccia levels (planar polarized light); f) Intrusive contact of the
798 Haggier pink granite in the doleritic basalt SP15A.
799
800 Fig. 5: A: Geological transect representing the studied area which correspond to a single bank
801 and location of the photographs B. B = Field photographs or microphotographs (scale bar =
802 2mm) or field sketch: a) Hornblende-bearing medium-grained diorites with stretching
803 lineation; b) Schematic illustration of microphotograph a; c) Alternating of sheets of tonalites
804 and diorites; d) Straight contact between tonalites and granodiorites; e) Mingling between
805 dioritic and granodioritic magmas; f) Vertical stretching lineation in diorites.
806
807 Fig. 6: Field photographs or microphotographs (scale bar = 2mm): a) Haggier layered gabbro;
808 b) Cpx+Pl+Ol layered gabbro (planar polarized light, Mont Haggier area); c) Intrusion of
809 granodiorites sills in the Sherubrub gabbros; d) Schematic illustration of photograph c.
810
811 Fig. 7: Field photographs or microphotographs (scale bar = 2mm): a) Sherubrub granite with
812 weak sub-solidus deformation (as = automorphic sphene, crossed polars); b) Protomylonitic
813 microstructure in Sherubrub granite (crossed polars); c) Amphibolitic rafts in pinkish
814 Sherubrub granite; d) Pegmatite swarm in gabbros at the periphery of the Sherubrub granite;
815 e) Quartz, zoned plagioclase and biotite in the Northern Haggier biotite granite (crossed
816 polars); f) Texture of the Haggier pink granite (planar polarized light).
817
818 Fig. 8: Field photographs or microphotographs (scale bar = 2mm): a) Magmatic breccia with
819 element of gabbro in Haggier pink granite matrix; b) Arfvedsonite (in blue) in the Haggier
820 pink granite (planar polarized light); c) Chessboard texture in quartz of the Haggier pink
821 granite (crossed polars); d) Basaltic dike intrusive in the Northern-Haggier Bt granite; e)
822 Doleritic texture in basaltic dikes formed mainly by hornblende and plagioclase; f) Rhyolitic
823 dikes intrusive in the Haggier layered gabbros.
824
825 Fig. 9: Stereogramms of dikes orientation in the Mont-Haggier area (Schmidt lower
826 hemisphere), a) Dikes of pinkish microgranite (36 measurements), b) Rhyolitic dikes (33), g)
827 Basaltic dikes (17).

Fig. 10: Total alkali silica diagram (LeBas et al., 1986) for magmatic rocks from Socotra Island. For the Mont-Haggier samples squares represent the mafic lavas and dikes, circles represent the granites and the triangle correspond to the basalt SP15A.

Fig. 11: A and B. Patterns of mafic cumulates and related volcanic and subvolcanic rocks from Mont-Haggier area normalised to Silicate Earth (McDonough and Sun, 1995) and Chondrites (Sun and McDonough, 1989), respectively. C. Patterns of diorites from Qalansya area and of the basalt SP15A from the Mont-Haggier area normalised to Silicate Earth (McDonough and Sun, 1995). D. Discrimination diagram (Cabanis and Lecolle, 1989) for subvolcanic to volcanic mafic rocks of Mont-Haggier area and the diorite of Qalantsya.

Fig. 12: A. ANK vs ACNK (Maniar and Piccoli, 1989) discrimination diagram for granitic bodies of Sherubrub area (grey circles) and Mont-Haggier area (dark circles). B. Patterns of granitic rocks from Socotra Island normalised to Silicate Earth (McDonough and Sun, 1995). C. Zr+Nb+Y+Ce vs 1000*Ga/Al diagram (Whalen et al., 1987) of granitic rocks from Socotra island. D. Discrimination diagram (Pearce et al., 1984) of granitic rocks from Socotra island.

Fig. 13: U-Pb concordia diagrams for (a) Haggier pink granite (sample HAEU-1), (b) gabbro enclaves in Haggier pink granite (sample HAEU-2) and (c) Sherubrub granite (sample SHEU-1).

Fig. 14: Interpretative block-diagram of the Mont-Haggier area.

Table 1: Major and trace elements compositions of selected magmatic rocks from Socotra island. < D.L. below detection limit. Mg#=100×MgO/(MgO+FeOTotal), on a molar basis.

Table 2: Analytic results of U-Pb dating using ion microprobe (CAMECA IMS 1270) on zircons from samples HAEU-1, HAEU-2 and SHEU-1.

862
863
864
865
866

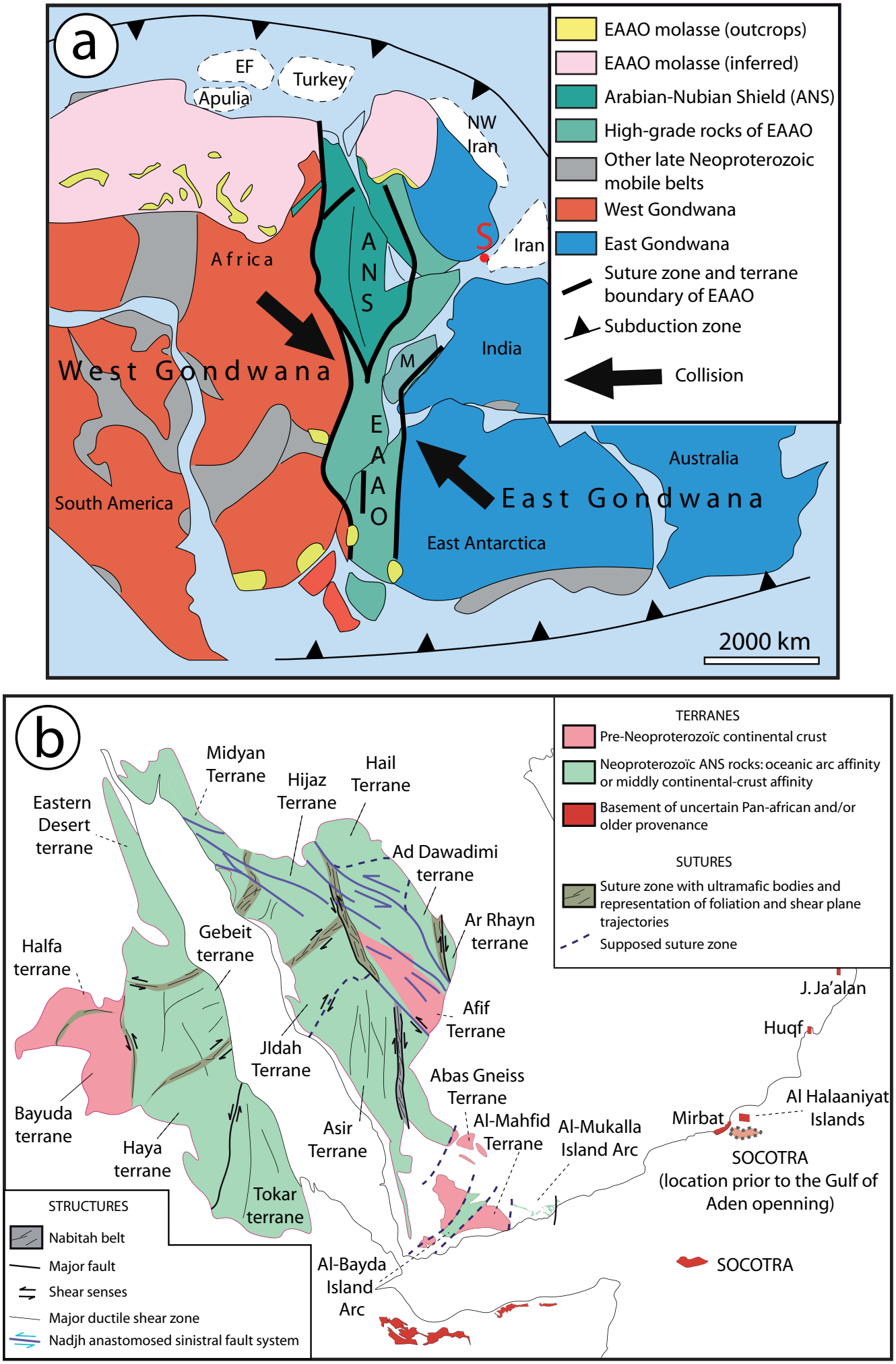
a
EF
Turkey
Apulia
NW
Iran
S
Iran
Africa
ANS
West Gondwana
M
India
EAAO
South America
Australia
East Gondwana
East Antarctica
2000 km
EAAO molasse (outcrops)
EAAO molasse (inferred)
Arabian-Nubian Shield (ANS)
High-grade rocks of EAAO
Other late Neoproterozoic mobile belts
West Gondwana
East Gondwana
Suture zone and terrane boundary of EAAO
Subduction zone
Collision
b
Midyan Terrane
Hijaz Terrane
Hail Terrane
Eastern Desert terrane
Ad Dawadimi terrane
Ar Rhayn terrane
Gebeit terrane
Halfa terrane
Afif Terrane
Jlidah Terrane
Abas Gneiss Terrane
Bayuda terrane
Asir Terrane
Al-Mahfid Terrane
Al-Mukalla Island Arc
Haya terrane
Tokar terrane
Al-Bayda Island Arc
J. Ja'alan
Huqf
Al Halaaniyat Islands
Mirbat
SOCOTRA
(location prior to the Gulf of Aden openning)
SOCOTRA
TERRANES
Pre-Neoproterozoïc continental crust
Neoproterozoïc ANS rocks: oceanic arc affinity or middly continental-crust affinity
Basement of uncertain Pan-african and/or older provenance
SUTURES
Suture zone with ultramafic bodies and representation of foliation and shear plane trajectories
Supposed suture zone
STRUCTURES
Nabitah belt
Major fault
Shear senses
Major ductile shear zone
Nadjh anastomosed sinistral fault system

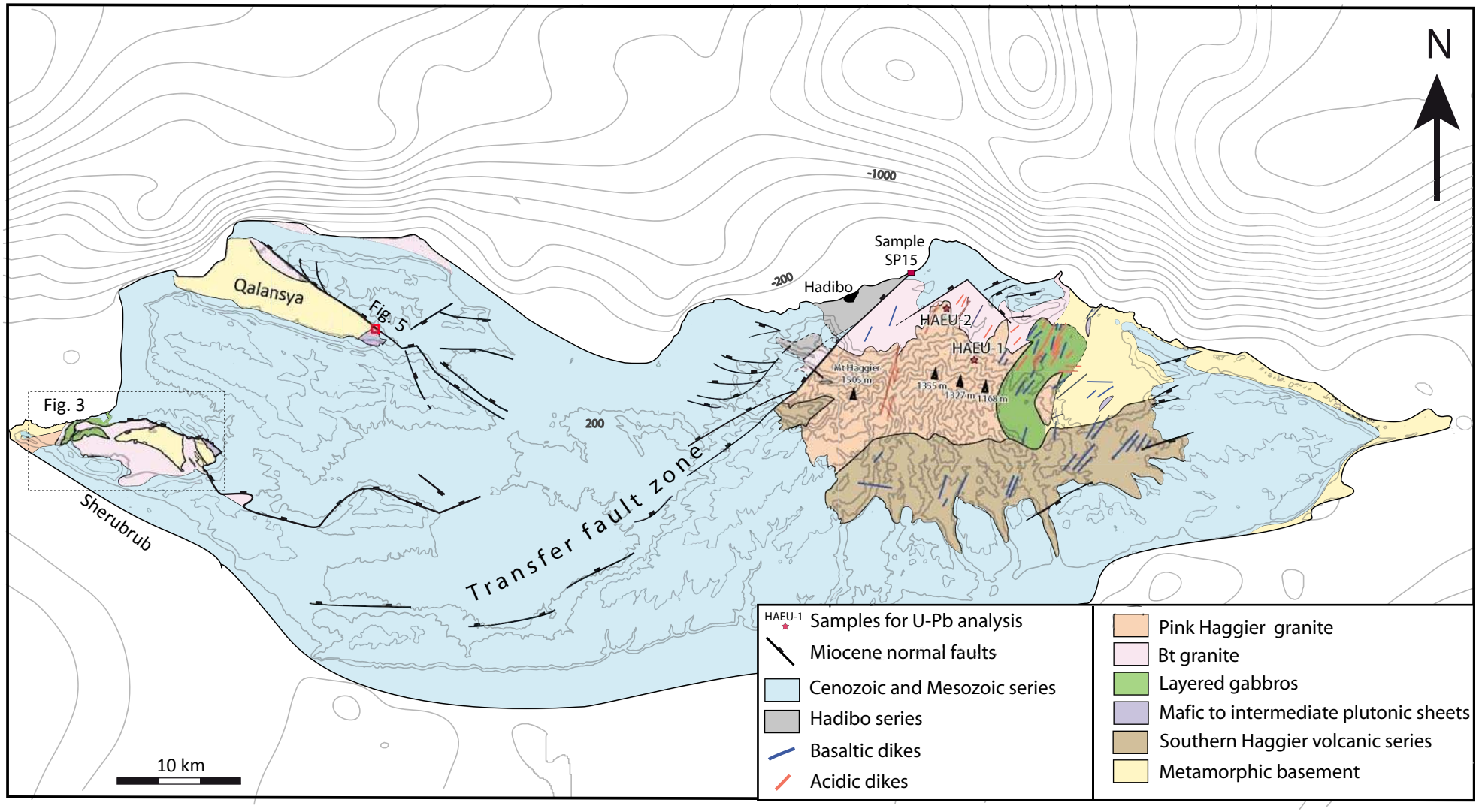
N
-1000
-200
200
Sample
SP15
Hadibo
HAEU-2
HAEU-1
Mt Haggier
1505 m
1355 m
1327 m
1168 m
Qalansya
Fig. 5
Fig. 3
Sherubrub
Transfer fault zone
10 km
HAEU-1 Samples for U-Pb analysis
Miocene normal faults
Cenozoic and Mesozoic series
Hadibo series
Basaltic dikes
Acidic dikes
Pink Haggier granite
Bt granite
Layered gabbros
Mafic to intermediate plutonic sheets
Southern Haggier volcanic series
Metamorphic basement

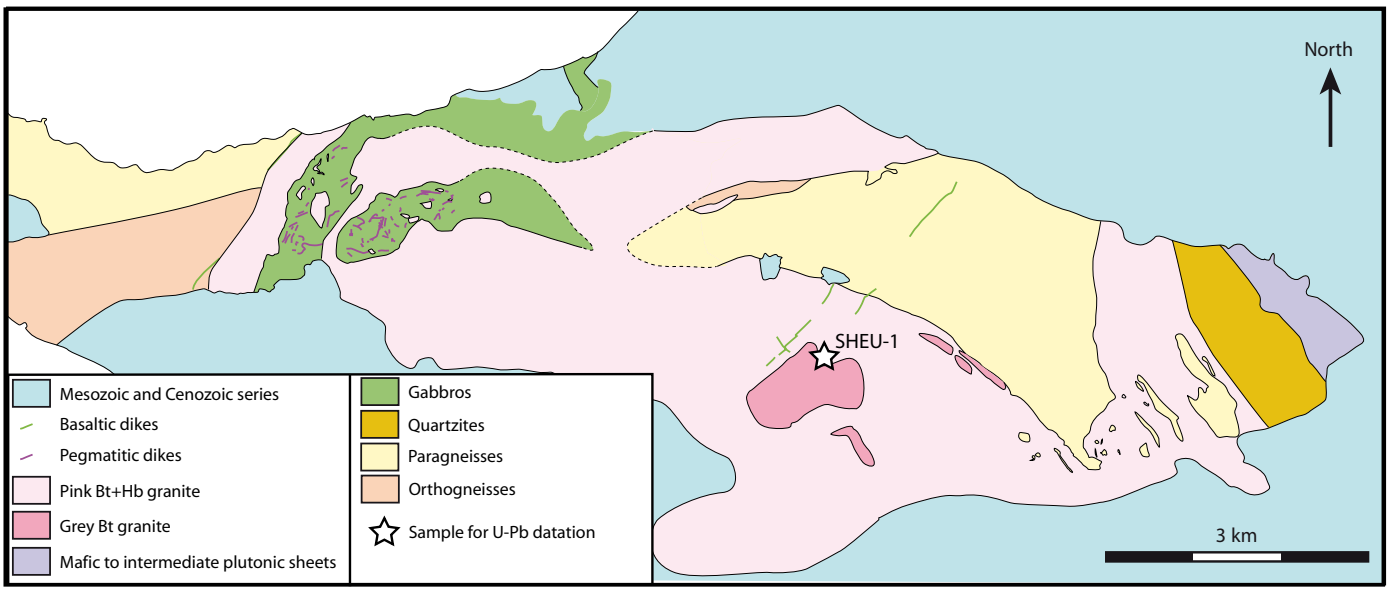
North
SHEU-1
3 km
Mesozoic and Cenozoic series
Basaltic dikes
Pegmatitic dikes
Pink Bt+Hb granite
Grey Bt granite
Mafic to intermediate plutonic sheets
Gabbros
Quartzites
Paragneisses
Orthogneisses
Sample for U-Pb datation

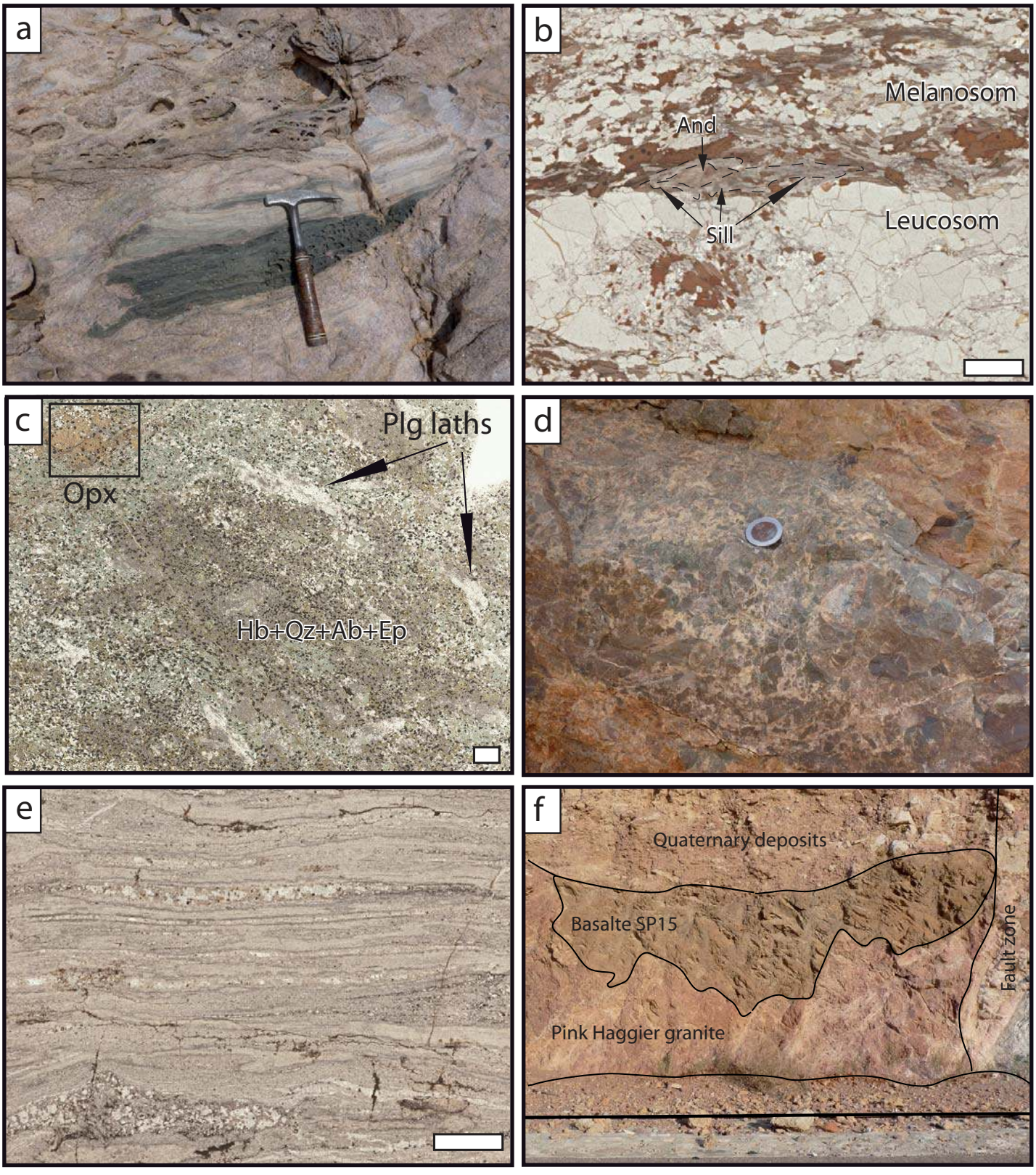
a
b
Melanosom
And
Sill
Leucosom
c
Opx
Plg laths
Hb+Qz+Ab+Ep
d
e
f
Quaternary deposits
Basalte SP15
Fault zone
Pink Haggier granite

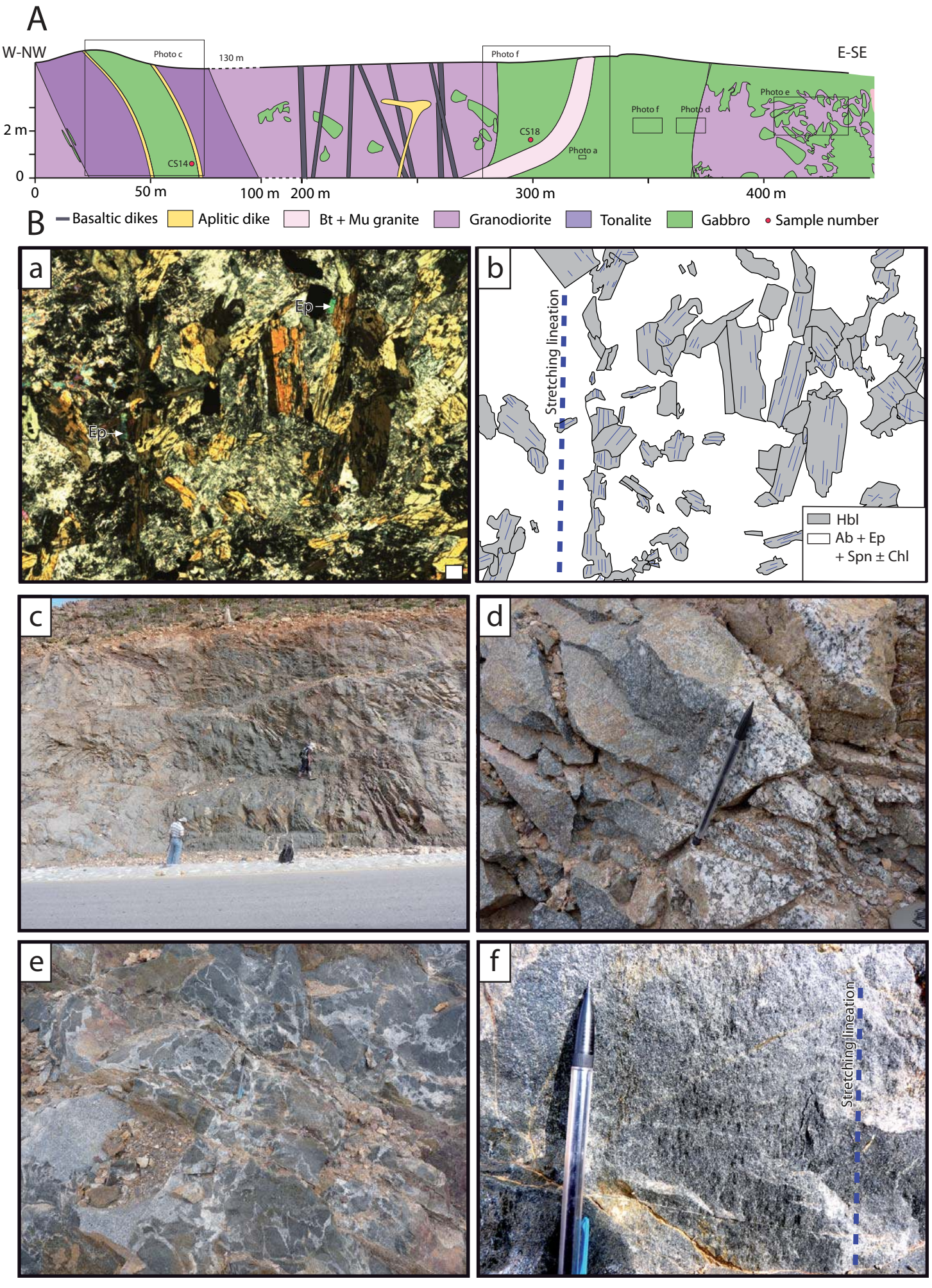
A
W-NW
E-SE
Photo c
130 m
Photo f
Photo e
Photo f
Photo d
CS18
Photo a
CS14
2 m
0
0
50 m
100 m
200 m
300 m
400 m
B
Basaltic dikes
Aplitic dike
Bt + Mu granite
Granodiorite
Tonalite
Gabbro
Sample number
a
Ep
Ep
b
Stretching lineation
Hbl
Ab + Ep
+ Spn ± Chl
c
d
e
f
Stretching lineation

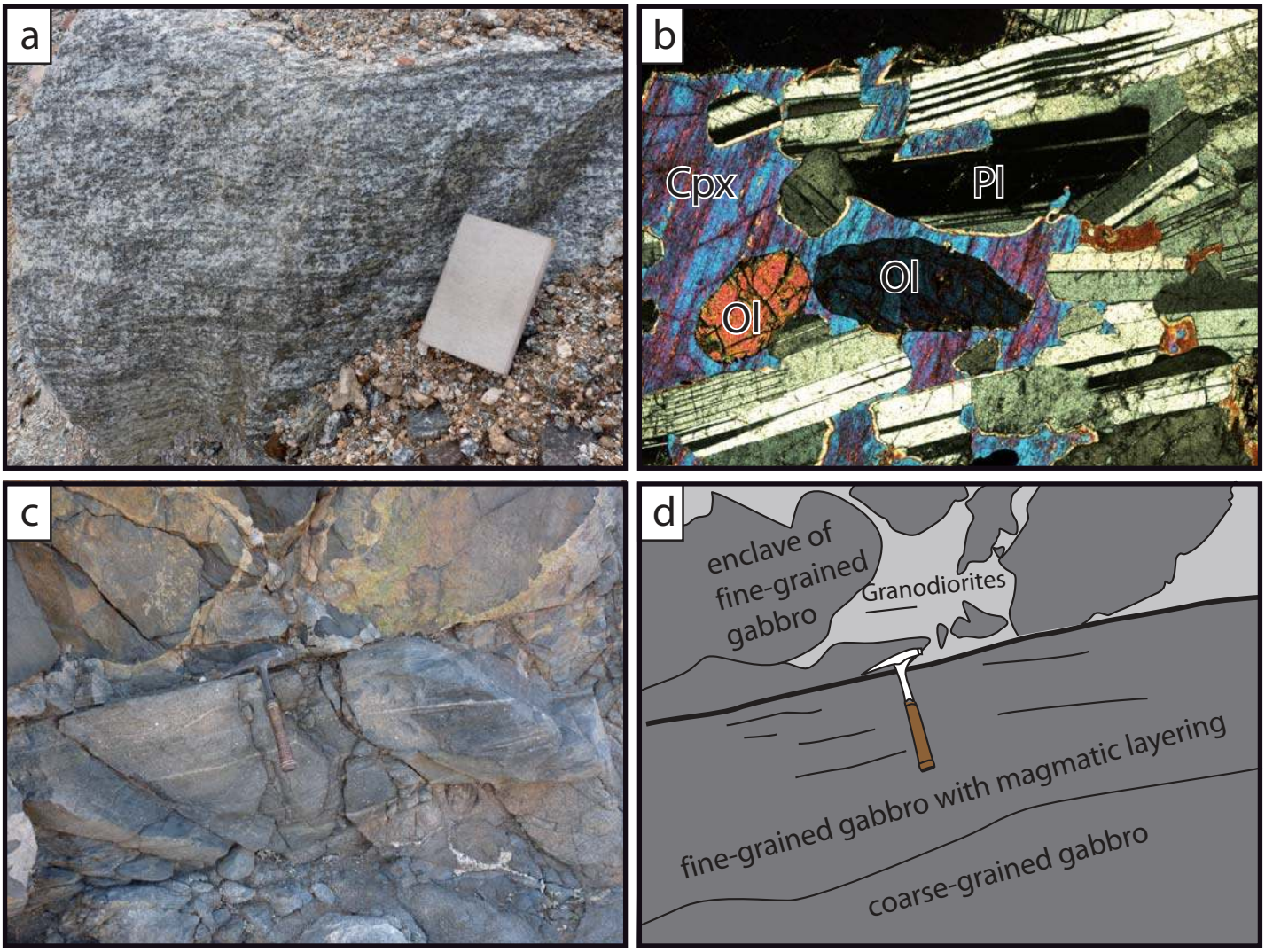
a
b
Cpx
Pl
Ol
Ol
c
d
enclave of fine-grained gabbro
Granodiorites
fine-grained gabbro with magmatic layering
coarse-grained gabbro

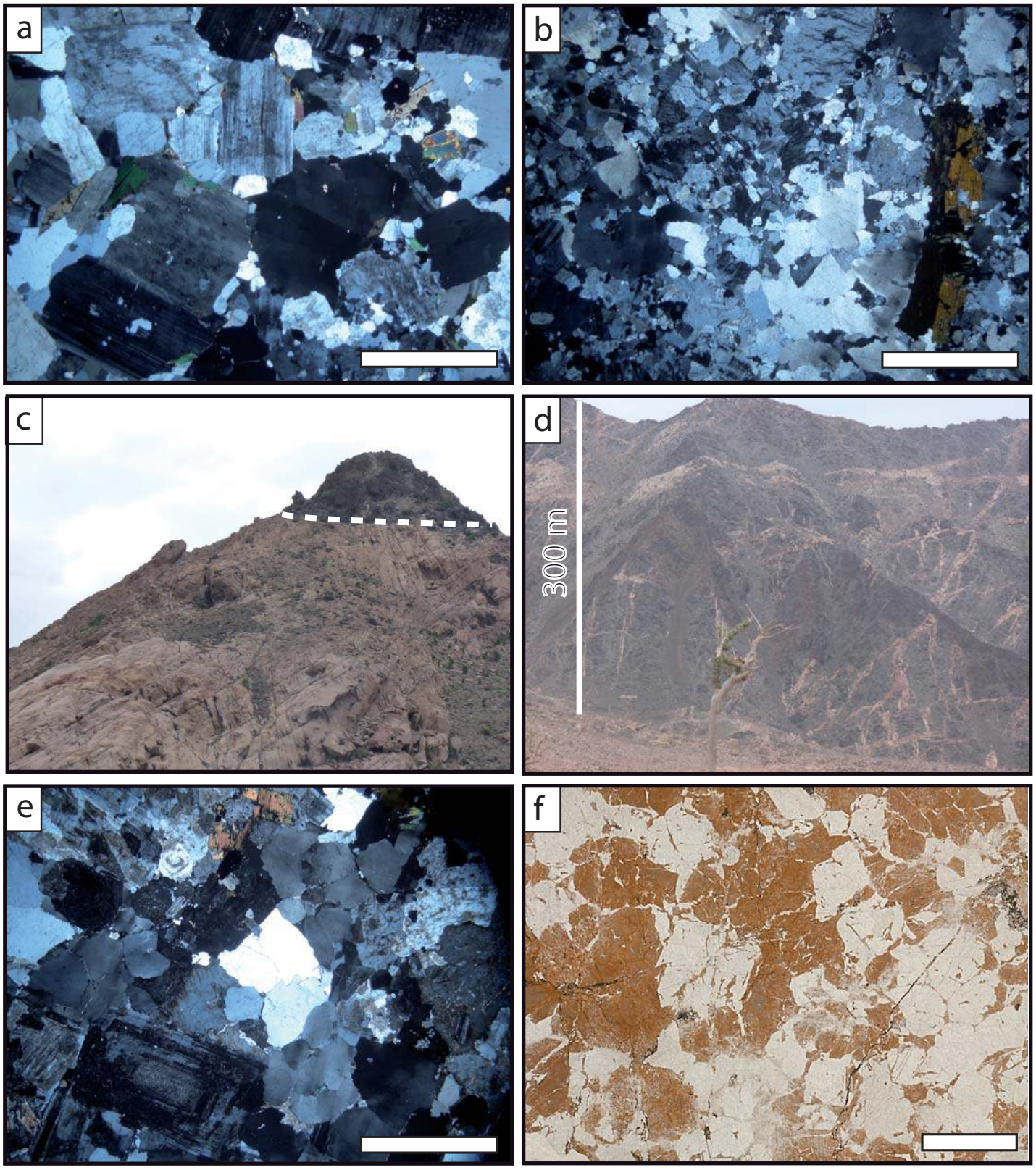
a
b
c
d
300 m
e
f

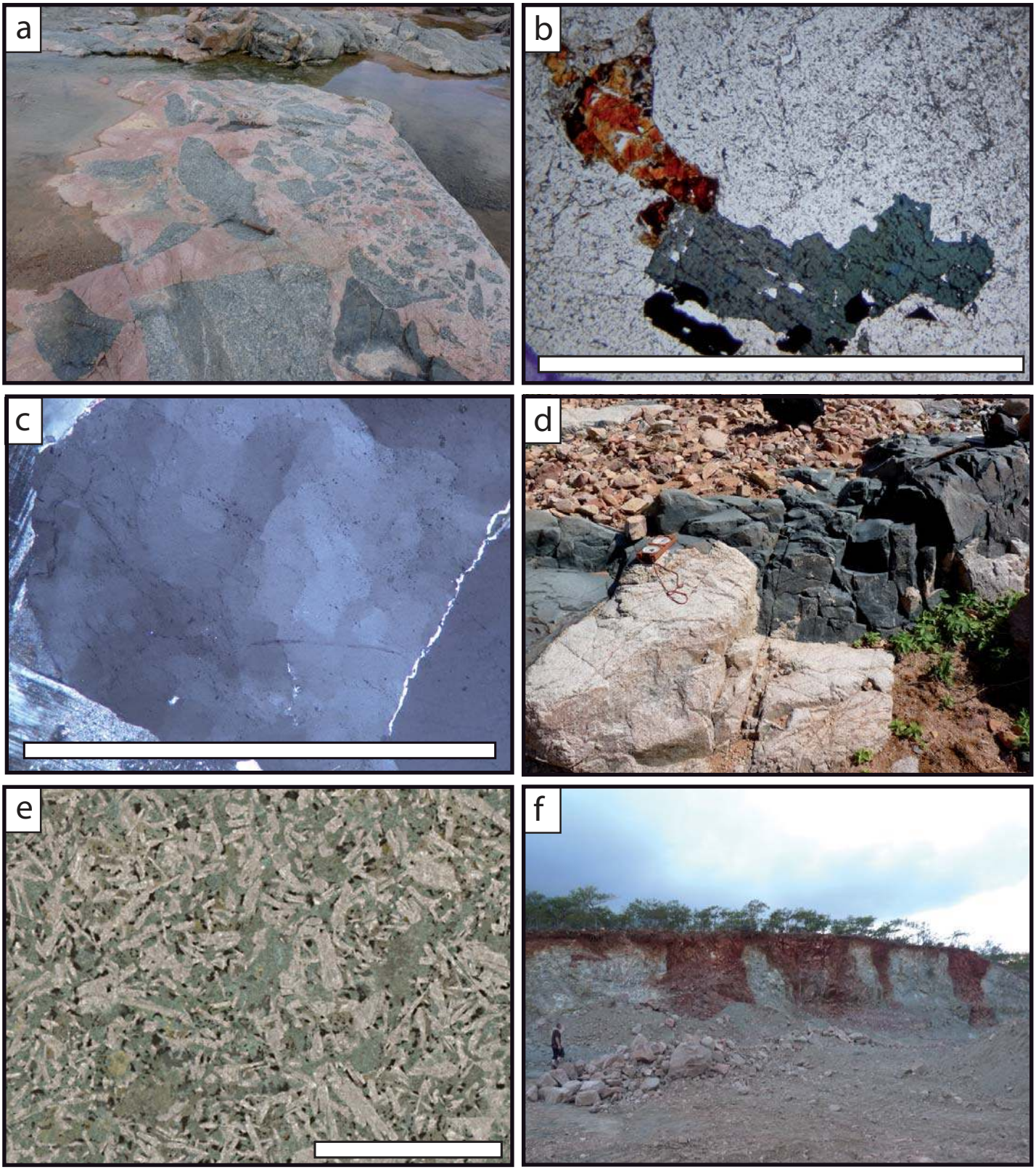
a
b
c
d
e
f

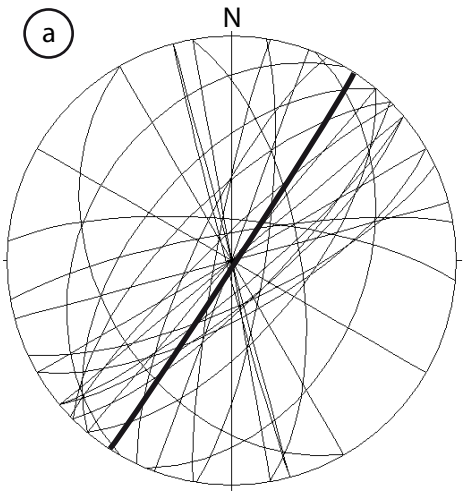

Mean plane = N33°E, S89

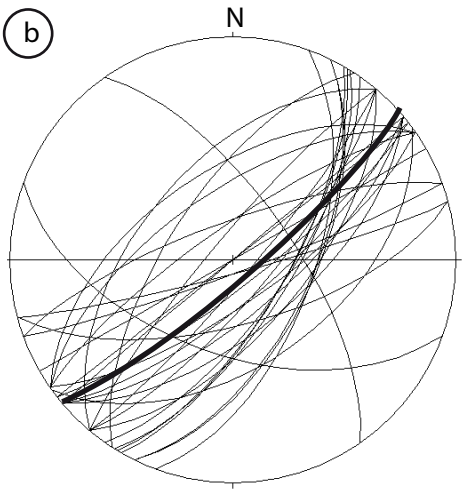

Mean plane = N59°E, S81

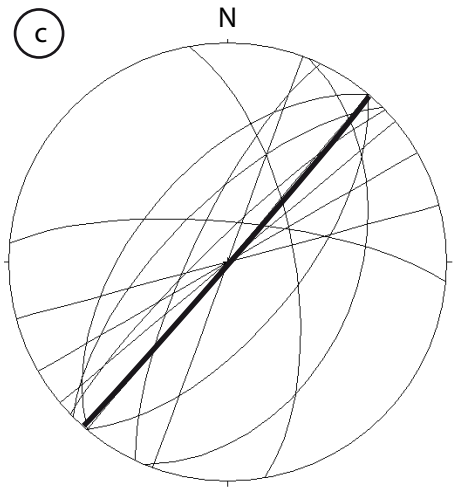

Mean plane = N41°E, S89

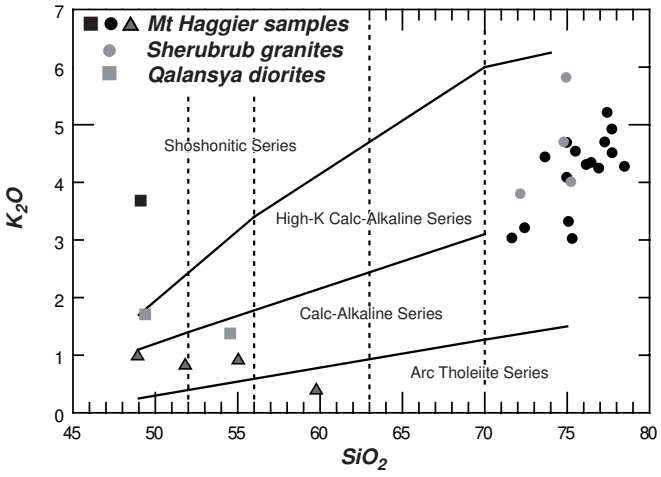
Mt Haggier samples
Sherubrub granites
Qalansya diorites
Shoshonitic Series
High-K Calc-Alkaline Series
Calc-Alkaline Series
Arc Tholeiite Series
K2O
SiO2
0
1
2
3
4
5
6
7
45
50
55
60
65
70
75
80

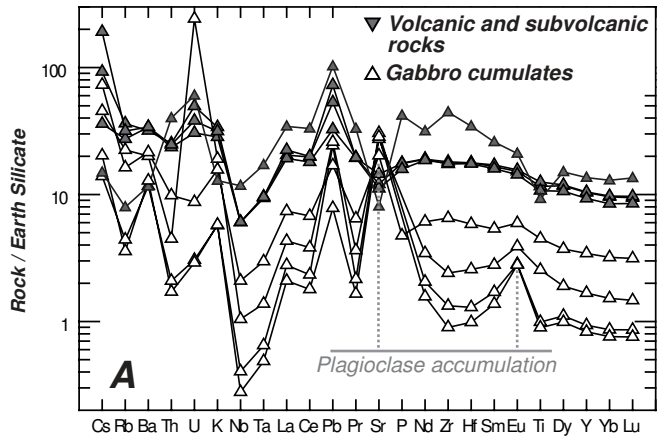
Volcanic and subvolcanic rocks
Gabbro cumulates
Rock / Earth Silicate
100
10
1
A
Plagioclase accumulation
Cs Rb Ba Th U K Nb Ta La Ce Pb Pr Sr P Nd Zr Hf Sm Eu Ti Dy Y Yb Lu

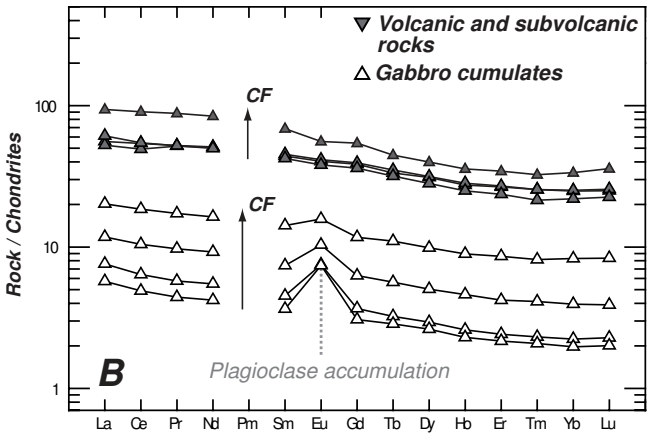
Volcanic and subvolcanic rocks
Gabbro cumulates
Rock / Chondrites
CF
CF
100
10
1
B
Plagioclase accumulation
La Ce Pr Nd Pm Sm Eu Gd Tb Dy Ho Er Tm Yb Lu

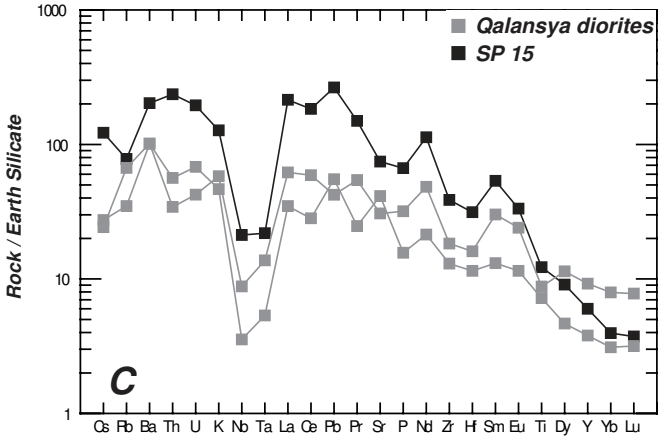
Qalansya diorites
SP 15
Rock / Earth Silicate
1000
100
10
1
C
Cs Rb Ba Th U K Nb Ta La Ce Pb Pr Sr P Nd Zr Hf Sm Eu Ti Dy Y Yb Lu

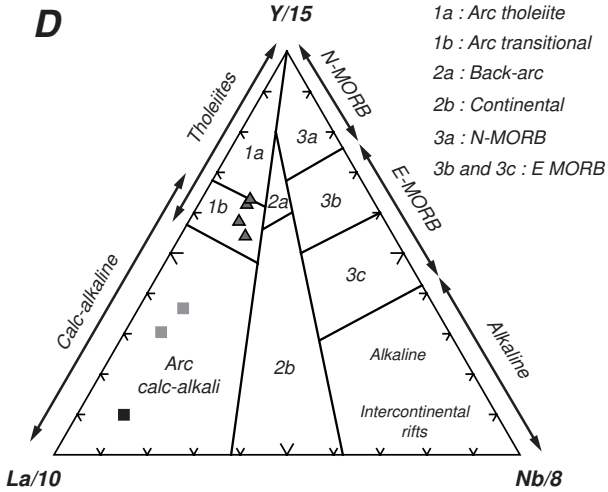
D
Y/15
La/10
Nb/8
Tholeiites
N-MORB
E-MORB
Calc-alkaline
Alkaline
1a
1b
2a
2b
3a
3b
3c
Arc calc-alkali
Alkaline
Intercontinental rifts
1a : Arc tholeiite
1b : Arc transitional
2a : Back-arc
2b : Continental
3a : N-MORB
3b and 3c : E MORB

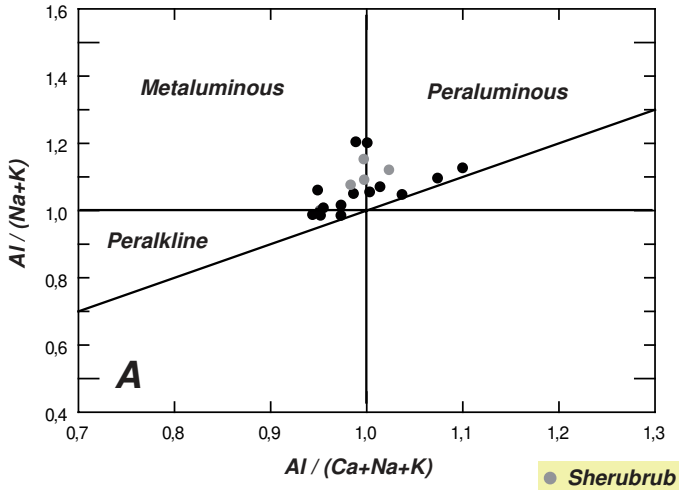

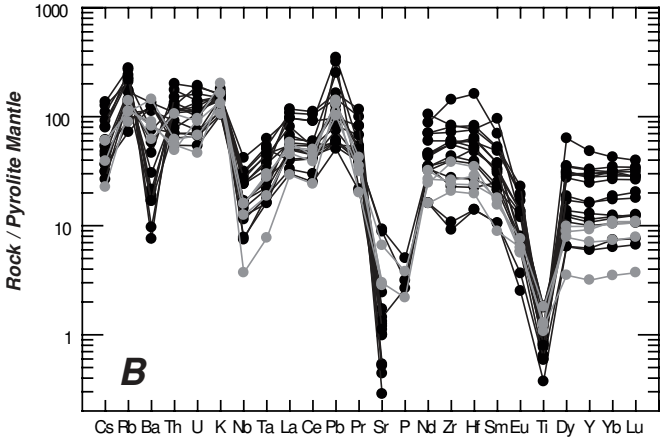

Sherubrub granites
Mt Haggier granites and felsic dikes

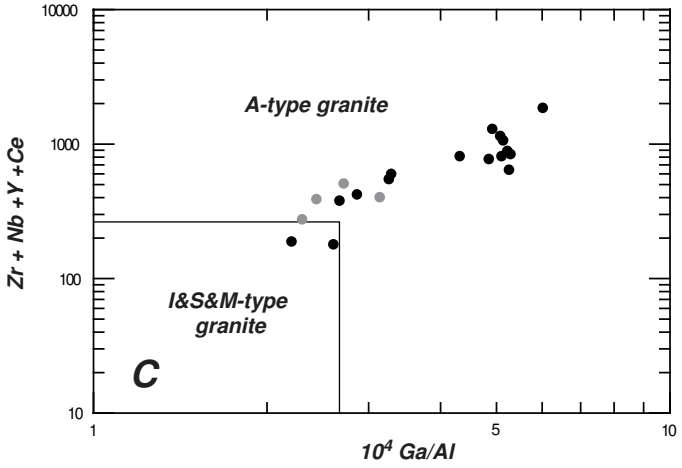

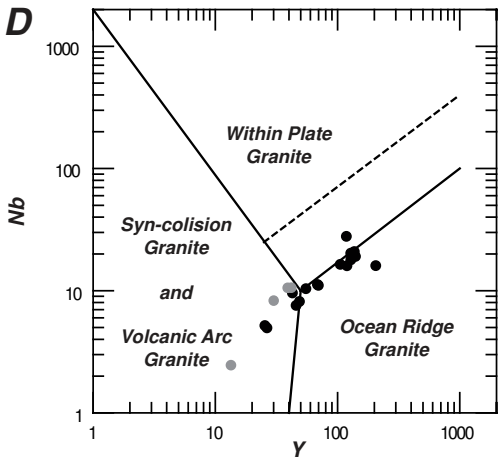

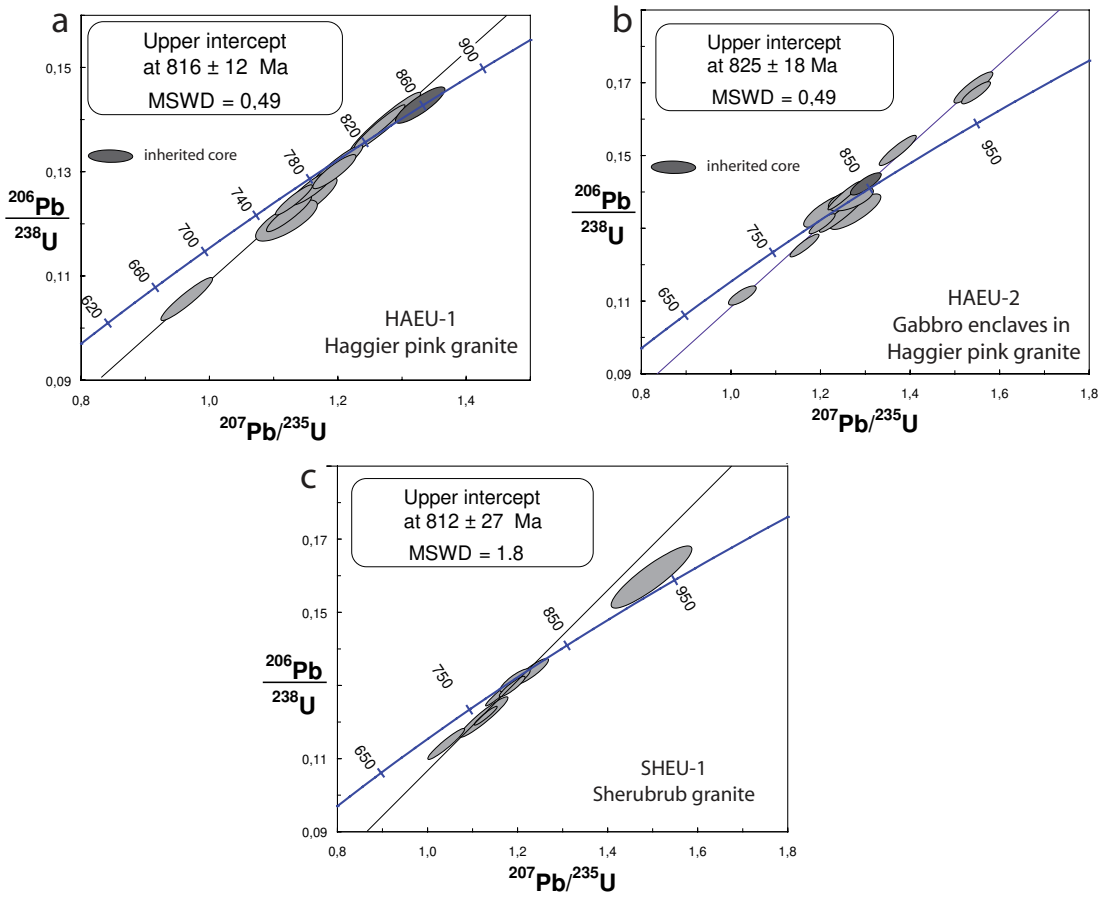
a
Upper intercept
at 816 ± 12 Ma
MSWD = 0,49
inherited core
HAEU-1
Haggier pink granite
b
Upper intercept
at 825 ± 18 Ma
MSWD = 0,49
inherited core
HAEU-2
Gabbro enclaves in
Haggier pink granite
C
Upper intercept
at 812 ± 27 Ma
MSWD = 1.8
SHEU-1
Sherubrub granite
206Pb/238U
207Pb/235U

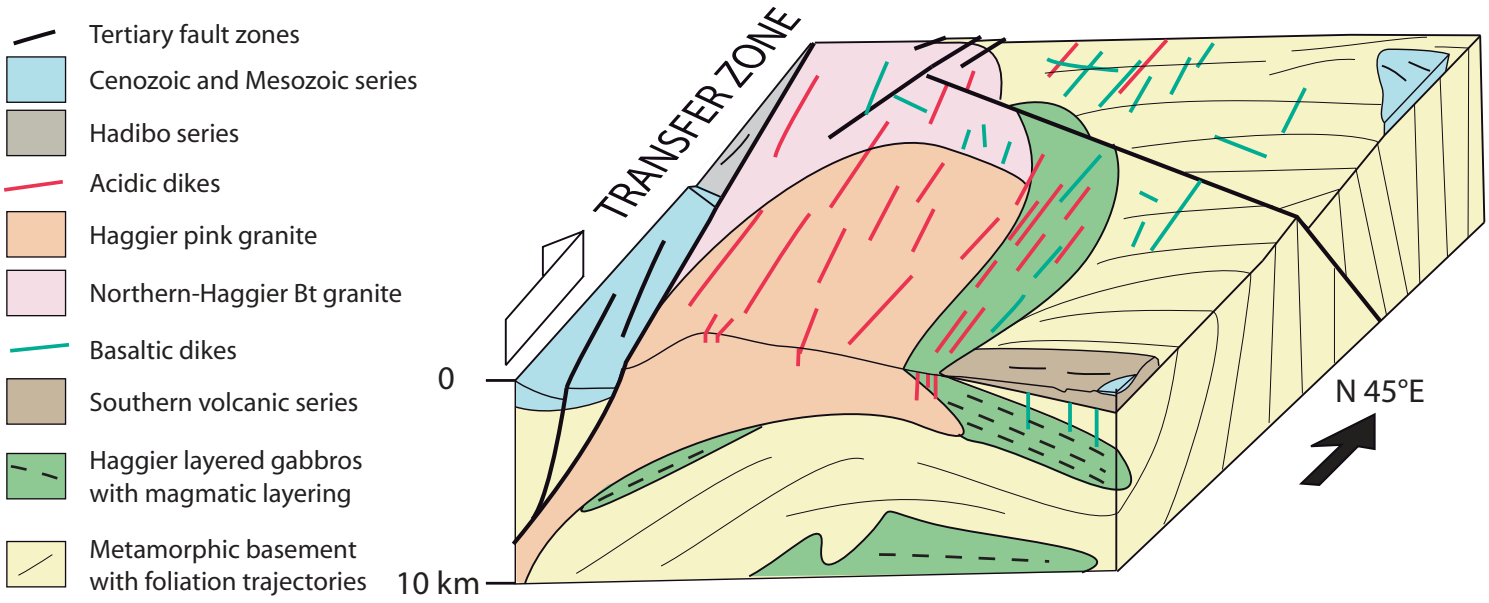
Tertiary fault zones
Cenozoic and Mesozoic series
Hadibo series
Acidic dikes
Haggier pink granite
Northern-Haggier Bt granite
Basaltic dikes
Southern volcanic series
Haggier layered gabbros with magmatic layering
Metamorphic basement with foliation trajectories
TRANSFER ZONE
0
10 km
N 45°E

Sample	SP10	SP16B	SP18	S20	S1	CS48A	S2	S5	SP15A	CS14A	CS18A	SP3	SP8B	CS45B	CS1A
Location	Haggier	Haggier	Haggier	Haggier	Haggier	Haggier	Haggier	Haggier	Haggier	Qalansya	Qalansya	Haggier	Haggier	Haggier	Haggier
Lithology	Mafic dike	Mafic tuff	Mafic dike	Basaltic lava	Gabbro cumulate	Gabbro cumulate	Gabbro cumulate	Gabbro cumulate	Altered basalt	Diorites	Diorites	Bt Granite	Bt Granite	Bt Granite	Bt Granite
%															
SiO2	48.92	55.04	51.82	59.86	48.09	50.94	49.63	51.10	49.11	49.38	54.55	71.67	75.11	73.68	72.45
Al2O3	14.31	13.52	14.60	10.64	26.32	23.26	21.08	17.30	15.31	16.94	17.21	13.89	12.88	11.72	14.34
Fe2O3t	13.03	11.59	13.99	11.21	2.71	4.10	5.53	7.80	8.86	11.15	8.48	2.15	1.99	3.47	1.90
MnO	0.32	0.26	0.25	0.24	0.04	0.06	0.08	0.13	0.13	0.20	0.13	0.11	0.07	0.07	0.08
MgO	2.86	2.43	3.07	2.89	3.70	3.66	7.55	6.72	3.15	4.08	4.40	0.53	0.08	0.05	0.43
CaO	8.33	6.42	6.69	5.20	14.78	12.78	11.95	10.68	6.01	6.92	7.33	1.27	0.34	0.29	1.42
Na2O	3.61	4.06	3.86	2.66	2.13	2.70	2.81	3.02	4.05	4.48	4.36	5.04	5.25	4.31	5.14
K2O	0.98	0.91	0.82	0.37	0.17	0.55	0.17	0.45	3.68	1.68	1.35	3.03	3.31	4.43	3.20
TiO2	2.33	2.15	2.52	1.86	0.20	0.51	0.18	0.90	2.46	1.76	1.45	0.37	0.16	0.25	0.36
P2O5	0.37	0.33	0.36	0.86	< D.L.	< D.L.	< D.L.	0.10	1.37	0.66	0.32	0.10	0.06	< D.L.	0.07
LOI	3.76	3.17	1.37	3.40	1.20	1.55	1.44	1.37	5.99	2.01	0.98	0.67	0.29	0.41	0.66
Total	98.82	99.88	99.35	99.18	99.34	100.11	100.41	99.57	100.13	99.26	100.55	98.83	99.55	98.68	100.03
ppm															
As	3	3	4	2	< D.L.	< D.L.	< D.L.	< D.L.	4	< D.L.	< D.L.	< D.L.	< D.L.	2	< D.L.
Ba	210	225	224	76	77	133	85	142	1338	670	669	821	816	307	744
Be	1.4	< D.L.	< D.L.	2.6	< D.L.	< D.L.	< D.L.	0.5	2.7	1.4	1.0	2.3	2.3	8.1	2.3
Bi	< D.L.	< D.L.	< D.L.	< D.L.	< D.L.	< D.L.	< D.L.	< D.L.	< D.L.	< D.L.	< D.L.	< D.L.	< D.L.	0.4	< D.L.
Cd	0.3	< D.L.	0.2	0.2	< D.L.	0.1	0.1	< D.L.	0.2	< D.L.	0.2	< D.L.	0.2	0.7	< D.L.
Co	27.7	23.5	28.5	16.4	15.0	18.2	40.5	38.1	21.3	24.7	25.2	1.5	0.7	< D.L.	1.4
Cr	18	15	18	0	211	88	165	123	27	< D.L.	52	6	6	4	6
Cs	1.9	4.0	0.8	0.3	0.3	1.0	0.4	1.5	2.6	0.5	0.6	1.0	0.7	1.1	1.3
Cu	29	12	23	8	38	24	108	78	61	154	55	< D.L.	< D.L.	26	17
Ga	20.4	19.4	24.1	23.2	18.5	18.5	16.6	18.5	25.8	20.4	20.6	21.1	22.2	31.9	20.3
Ge	1.7	1.5	1.9	2.6	0.9	1.0	0.9	1.3	1.6	1.4	1.2	1.7	1.8	2.4	1.7
Hf	4.99	4.88	4.97	9.65	0.36	0.72	0.28	1.64	8.77	4.49	3.21	7.47	10.35	21.28	6.29
In	0.10	< D.L.	0.11	< D.L.	< D.L.	< D.L.	< D.L.	< D.L.	< D.L.	< D.L.	< D.L.	< D.L.	0.12	0.25	< D.L.
Mo	0.8	0.7	1.1	0.6	0.6	2.9	0.0	0.4	0.6	0.7	0.4	0.4	0.6	1.5	0.7
Nb	4.0	4.0	4.0	7.7	0.3	0.7	0.2	1.4	14.0	5.8	2.3	9.5	7.5	27.6	10.3
Ni	10	8	7	< D.L.	73	30	122	50	16	< D.L.	35	< D.L.	< D.L.	< D.L.	< D.L.
Pb	8	11	5	15	4	4	1	3	40	6	8	9	8	52	11
Rb	22	19	16	5	3	13	2	10	47	40	21	56	55	104	66
Sb	0.2	0.7	0.2	0.8	< D.L.	0.1	< D.L.	< D.L.	0.4	< D.L.	< D.L.	< D.L.	< D.L.	0.5	0.1
Sn	2.1	1.7	2.0	2.4	< D.L.	1.0	< D.L.	0.6	3.2	3.0	1.1	2.6	3.0	15.3	3.8
Sr	240	222	289	161	607	544	566	404	1484	610	823	184	29	11	176
Ta	0.36	0.35	0.35	0.63	0.02	0.05	0.02	0.11	0.81	0.51	0.20	0.80	0.68	2.32	1.04
Th	2.01	1.96	1.87	3.18	0.17	0.36	0.14	0.78	18.78	2.73	4.48	5.04	5.64	13.97	7.28
U	1.01	0.77	0.62	1.22	0.06	4.91	0.06	0.18	3.96	0.86	1.38	1.35	1.38	2.83	1.52
V	280	240	289	71	45	102	50	172	207	181	184	14	2	1	14
W	0.42	0.60	< D.L.	0.74	< D.L.	0.33	< D.L.	< D.L.	0.33	< D.L.	< D.L.	< D.L.	< D.L.	0.94	0.22
Y	44.5	40.0	45.0	58.4	4.0	7.2	3.6	14.8	25.8	39.7	16.3	43.1	46.3	119.1	55.6
Zn	130	126	131	161	20	35	39	68	171	115	105	70	76	314	66
Zr	182	184	190	467	14	25	9	68	406	192	136	289	416	755	240
La	13.2	14.5	12.5	22.3	1.8	2.8	1.4	4.8	139.0	40.1	22.6	32.7	32.2	63.0	26.4
Ce	33.1	33.4	30.2	55.5	3.9	6.4	3.0	11.4	307.7	98.9	47.3	76.4	74.5	153.7	70.4
Pr	4.96	4.95	4.92	8.38	0.55	0.92	0.42	1.64	38.00	13.80	6.28	10.14	9.78	20.86	10.27
Nd	23.86	23.28	23.66	39.40	2.57	4.31	1.97	7.64	141.20	60.51	26.73	41.52	40.09	87.48	43.52
Sm	6.73	6.48	6.94	10.52	0.69	1.13	0.56	2.17	21.76	12.24	5.32	8.70	8.62	20.87	10.15
Eu	2.34	2.21	2.41	3.24	0.44	0.60	0.43	0.92	5.14	3.70	1.77	1.90	1.06	3.03	2.00
Gd	7.91	7.43	8.10	11.16	0.76	1.29	0.63	2.41	11.94	9.86	4.26	7.43	8.07	20.33	9.20
Tb	1.25	1.19	1.31	1.67	0.12	0.21	0.11	0.41	1.39	1.35	0.57	1.19	1.33	3.37	1.50
Dy	7.89	7.15	8.01	10.14	0.75	1.28	0.67	2.51	6.12	7.67	3.14	7.32	8.15	20.63	9.29
Ho	1.55	1.42	1.60	2.02	0.15	0.26	0.13	0.51	0.90	1.42	0.57	1.44	1.62	4.18	1.86
Er	4.41	3.91	4.47	5.70	0.40	0.70	0.36	1.42	2.21	3.82	1.52	4.25	4.74	12.27	5.36
Tm	0.65	0.55	0.65	0.83	0.06	0.11	0.05	0.21	0.29	0.54	0.22	0.67	0.74	1.95	0.83
Yb	4.23	3.73	4.29	5.71	0.38	0.67	0.34	1.41	1.74	3.50	1.37	4.61	5.16	14.02	5.49
Lu	0.64	0.57	0.65	0.91	0.06	0.10	0.05	0.21	0.25	0.53	0.21	0.72	0.84	2.24	0.82
ΣREE	112.8	110.8	109.6	177.4	12.6	20.8	10.1	37.6	677.6	258.0	121.8	199.0	196.9	427.9	197.1
Mg#	17	17	17	20	56	46	56	45	25	26	33	19	4	1	18
Ce/Yb	8	9	7	10	10	10	9	8	176	28	35	17	14	11	13
La_N/Nb_N	3.4	3.7	3.2	2.9	6.9	4.1	7.5	3.5	10.1	7.0	9.8	3.5	4.3	2.3	2.6

Sample	SP10	SP16B	SP18	S20	S1	CS48A	S2	S5	SP15A	CS14A	CS18A	SP3	SP8B	CS45B	CS1A
Location	Haggier	Haggier	Haggier	Haggier	Haggier	Haggier	Haggier	Haggier	Haggier	Qalansya	Qalansya	Haggier	Haggier	Haggier	Haggier
Lithology	Mafic dike	Mafic tuff	Mafic dike	Basaltic lava	Gabbro cumulate	Gabbro cumulate	Gabbro cumulate	Gabbro cumulate	Altered basalt	Diorites	Diorites	Bt Granite	Bt Granite	Bt Granite	Bt Granite
%															
SiO2	48.92	55.04	51.82	59.86	48.09	50.94	49.63	51.10	49.11	49.38	54.55	71.67	75.11	73.68	72.45
Al2O3	14.31	13.52	14.60	10.64	26.32	23.26	21.08	17.30	15.31	16.94	17.21	13.89	12.88	11.72	14.34
Fe2O3t	13.03	11.59	13.99	11.21	2.71	4.10	5.53	7.80	8.86	11.15	8.48	2.15	1.99	3.47	1.90
MnO	0.32	0.26	0.25	0.24	0.04	0.06	0.08	0.13	0.13	0.20	0.13	0.11	0.07	0.07	0.08
MgO	2.86	2.43	3.07	2.89	3.70	3.66	7.55	6.72	3.15	4.08	4.40	0.53	0.08	0.05	0.43
CaO	8.33	6.42	6.69	5.20	14.78	12.78	11.95	10.68	6.01	6.92	7.33	1.27	0.34	0.29	1.42
Na2O	3.61	4.06	3.86	2.66	2.13	2.70	2.81	3.02	4.05	4.48	4.36	5.04	5.25	4.31	5.14
K2O	0.98	0.91	0.82	0.37	0.17	0.55	0.17	0.45	3.68	1.68	1.35	3.03	3.31	4.43	3.20
TiO2	2.33	2.15	2.52	1.86	0.20	0.51	0.18	0.90	2.46	1.76	1.45	0.37	0.16	0.25	0.36
P2O5	0.37	0.33	0.36	0.86	< D.L.	< D.L.	< D.L.	0.10	1.37	0.66	0.32	0.10	0.06	< D.L.	0.07
LOI	3.76	3.17	1.37	3.40	1.20	1.55	1.44	1.37	5.99	2.01	0.98	0.67	0.29	0.41	0.66
Total	98.82	99.88	99.35	99.18	99.34	100.11	100.41	99.57	100.13	99.26	100.55	98.83	99.55	98.68	100.03
ppm															
As	3	3	4	2	< D.L.	< D.L.	< D.L.	< D.L.	4	< D.L.	< D.L.	< D.L.	< D.L.	2	< D.L.
Ba	210	225	224	76	77	133	85	142	1338	670	669	821	816	307	744
Be	1.4	< D.L.	< D.L.	2.6	< D.L.	< D.L.	< D.L.	0.5	2.7	1.4	1.0	2.3	2.3	8.1	2.3
Bi	< D.L.	< D.L.	< D.L.	< D.L.	< D.L.	< D.L.	< D.L.	< D.L.	< D.L.	< D.L.	< D.L.	< D.L.	< D.L.	0.4	< D.L.
Cd	0.3	< D.L.	0.2	0.2	< D.L.	0.1	0.1	< D.L.	0.2	< D.L.	0.2	< D.L.	0.2	0.7	< D.L.
Co	27.7	23.5	28.5	16.4	15.0	18.2	40.5	38.1	21.3	24.7	25.2	1.5	0.7	< D.L.	1.4
Cr	18	15	18	0	211	88	165	123	27	< D.L.	52	6	6	4	6
Cs	1.9	4.0	0.8	0.3	0.3	1.0	0.4	1.5	2.6	0.5	0.6	1.0	0.7	1.1	1.3
Cu	29	12	23	8	38	24	108	78	61	154	55	< D.L.	< D.L.	26	17
Ga	20.4	19.4	24.1	23.2	18.5	18.5	16.6	18.5	25.8	20.4	20.6	21.1	22.2	31.9	20.3
Ge	1.7	1.5	1.9	2.6	0.9	1.0	0.9	1.3	1.6	1.4	1.2	1.7	1.8	2.4	1.7
Hf	4.99	4.88	4.97	9.65	0.36	0.72	0.28	1.64	8.77	4.49	3.21	7.47	10.35	21.28	6.29
In	0.10	< D.L.	0.11	< D.L.	< D.L.	< D.L.	< D.L.	< D.L.	< D.L.	< D.L.	< D.L.	< D.L.	0.12	0.25	< D.L.
Mo	0.8	0.7	1.1	0.6	0.6	2.9	0.0	0.4	0.6	0.7	0.4	0.4	0.6	1.5	0.7
Nb	4.0	4.0	4.0	7.7	0.3	0.7	0.2	1.4	14.0	5.8	2.3	9.5	7.5	27.6	10.3
Ni	10	8	7	< D.L.	73	30	122	50	16	< D.L.	35	< D.L.	< D.L.	< D.L.	< D.L.
Pb	8	11	5	15	4	4	1	3	40	6	8	9	8	52	11
Rb	22	19	16	5	3	13	2	10	47	40	21	56	55	104	66
Sb	0.2	0.7	0.2	0.8	< D.L.	0.1	< D.L.	< D.L.	0.4	< D.L.	< D.L.	< D.L.	< D.L.	0.5	0.1
Sn	2.1	1.7	2.0	2.4	< D.L.	1.0	< D.L.	0.6	3.2	3.0	1.1	2.6	3.0	15.3	3.8
Sr	240	222	289	161	607	544	566	404	1484	610	823	184	29	11	176
Ta	0.36	0.35	0.35	0.63	0.02	0.05	0.02	0.11	0.81	0.51	0.20	0.80	0.68	2.32	1.04
Th	2.01	1.96	1.87	3.18	0.17	0.36	0.14	0.78	18.78	2.73	4.48	5.04	5.64	13.97	7.28
U	1.01	0.77	0.62	1.22	0.06	4.91	0.06	0.18	3.96	0.86	1.38	1.35	1.38	2.83	1.52
V	280	240	289	71	45	102	50	172	207	181	184	14	2	1	14
W	0.42	0.60	< D.L.	0.74	< D.L.	0.33	< D.L.	< D.L.	0.33	< D.L.	< D.L.	< D.L.	< D.L.	0.94	0.22
Y	44.5	40.0	45.0	58.4	4.0	7.2	3.6	14.8	25.8	39.7	16.3	43.1	46.3	119.1	55.6
Zn	130	126	131	161	20	35	39	68	171	115	105	70	76	314	66
Zr	182	184	190	467	14	25	9	68	406	192	136	289	416	755	240
La	13.2	14.5	12.5	22.3	1.8	2.8	1.4	4.8	139.0	40.1	22.6	32.7	32.2	63.0	26.4
Ce	33.1	33.4	30.2	55.5	3.9	6.4	3.0	11.4	307.7	98.9	47.3	76.4	74.5	153.7	70.4
Pr	4.96	4.95	4.92	8.38	0.55	0.92	0.42	1.64	38.00	13.80	6.28	10.14	9.78	20.86	10.27
Nd	23.86	23.28	23.66	39.40	2.57	4.31	1.97	7.64	141.20	60.51	26.73	41.52	40.09	87.48	43.52
Sm	6.73	6.48	6.94	10.52	0.69	1.13	0.56	2.17	21.76	12.24	5.32	8.70	8.62	20.87	10.15
Eu	2.34	2.21	2.41	3.24	0.44	0.60	0.43	0.92	5.14	3.70	1.77	1.90	1.06	3.03	2.00
Gd	7.91	7.43	8.10	11.16	0.76	1.29	0.63	2.41	11.94	9.86	4.26	7.43	8.07	20.33	9.20
Tb	1.25	1.19	1.31	1.67	0.12	0.21	0.11	0.41	1.39	1.35	0.57	1.19	1.33	3.37	1.50
Dy	7.89	7.15	8.01	10.14	0.75	1.28	0.67	2.51	6.12	7.67	3.14	7.32	8.15	20.63	9.29
Ho	1.55	1.42	1.60	2.02	0.15	0.26	0.13	0.51	0.90	1.42	0.57	1.44	1.62	4.18	1.86
Er	4.41	3.91	4.47	5.70	0.40	0.70	0.36	1.42	2.21	3.82	1.52	4.25	4.74	12.27	5.36
Tm	0.65	0.55	0.65	0.83	0.06	0.11	0.05	0.21	0.29	0.54	0.22	0.67	0.74	1.95	0.83
Yb	4.23	3.73	4.29	5.71	0.38	0.67	0.34	1.41	1.74	3.50	1.37	4.61	5.16	14.02	5.49
Lu	0.64	0.57	0.65	0.91	0.06	0.10	0.05	0.21	0.25	0.53	0.21	0.72	0.84	2.24	0.82
ΣREE	112.8	110.8	109.6	177.4	12.6	20.8	10.1	37.6	677.6	258.0	121.8	199.0	196.9	427.9	197.1
Mg#	17	17	17	20	56	46	56	45	25	26	33	19	4	1	18
Ce/Yb	8	9	7	10	10	10	9	8	176	28	35	17	14	11	13
La_N/Nb_N	3.4	3.7	3.2	2.9	6.9	4.1	7.5	3.5	10.1	7.0	9.8	3.5	4.3	2.3	2.6

		Contents (ppm)				Measured	% Pbc	Corrected ratios							Ages (Ma)			
Echantillon	Domain	Pb	U	Th	Th/U	$^{204}Pb/^{206}Pb$		$^{207}Pb/^{206}Pb$	± σ	$^{206}Pb/^{238}U$	± σ	$^{207}Pb/^{235}U$	± σ	Err. Corr	$^{206}Pb/^{238}U$	± σ	$^{207}Pb/^{235}U$	± σ
HAEU1-a	Core	5	44	34	0.77	2.46E-04	0.23%	0.0667	0.0204	0.1379	0.0022	1.2680	0.0329	0.62	833	13	831	15
HAEU1-a	Rim	6	52	41	0.79	1.04E-04	0.00%	0.0690	0.0171	0.1344	0.0032	1.2779	0.0378	0.82	813	18	836	17
HAEU1-b	Core	47	394	416	1.06	1.70E-05	0.00%	0.0655	0.0058	0.1388	0.0025	1.2534	0.0240	0.95	838	14	825	11
HAEU1-b	Rim	52	452	432	0.95	3.28E-04	0.54%	0.0653	0.0156	0.1346	0.0030	1.2121	0.0326	0.82	814	17	806	15
HAEU1-c	Core	18	159	145	0.92	6.67E-05	0.04%	0.0666	0.0079	0.1311	0.0018	1.2038	0.0193	0.87	794	10	802	9
HAEU1-d	Core	18	123	109	0.89	5.50E-05	0.03%	0.0663	0.0083	0.1686	0.0028	1.5412	0.0288	0.90	1005	16	947	11
HAEU1-d	Rim	41	315	387	1.23	4.29E-05	0.04%	0.0658	0.0081	0.1513	0.0028	1.3719	0.0274	0.91	908	15	877	12
HAEU1-e	Core	25	177	233	1.32	3.05E-05	0.00%	0.0671	0.0068	0.1672	0.0020	1.5474	0.0215	0.87	997	11	949	9
HAEU1-e	Rim	44	407	673	1.65	1.97E-04	0.31%	0.0675	0.0081	0.1251	0.0021	1.1645	0.0215	0.90	760	12	784	10
HAEU1-f	Rim	17	175	199	1.14	1.39E-04	0.15%	0.0669	0.0123	0.1113	0.0017	1.0257	0.0204	0.79	680	10	717	10
HAEU1-f	Core	27	222	274	1.23	1.29E-04	0.17%	0.0664	0.0097	0.1421	0.0020	1.3012	0.0226	0.83	856	12	846	10
HAEU2-a	Core	17	146	85	0.58	1.53E-05	0.00%	0.0662	0.0054	0.1387	0.0027	1.2654	0.0257	0.96	837	15	830	11
HAEU2-a	Rim	12	116	58	0.50	4.51E-05	0.03%	0.0659	0.0060	0.1245	0.0019	1.1317	0.0187	0.93	756	11	769	9
HAEU2-b	Core	14	133	75	0.56	1.03E-04	0.13%	0.0671	0.0138	0.1242	0.0030	1.1496	0.0323	0.87	755	17	777	15
HAEU2-b	Rim	15	170	76	0.45	1.43E-04	0.20%	0.0664	0.0097	0.1054	0.0027	0.9645	0.0266	0.94	646	16	686	14
HAEU2-c	Core	11	103	48	0.47	2.22E-04	0.32%	0.0674	0.0184	0.1205	0.0026	1.1202	0.0318	0.76	734	15	763	15
HAEU2-d	Core	10	80	40	0.50	9.80E-05	0.09%	0.0675	0.0099	0.1427	0.0023	1.3284	0.0252	0.85	860	13	858	11
HAEU2-d	Rim	13	112	58	0.51	6.50E-05	0.05%	0.0663	0.0079	0.1394	0.0038	1.2744	0.0363	0.96	841	22	834	16
HAEU2-e	Core	13	115	61	0.53	1.10E-04	0.13%	0.0664	0.0083	0.1309	0.0027	1.1981	0.0268	0.93	793	15	800	12
HAEU2-e	Rim	13	120	61	0.51	9.22E-05	0.09%	0.0667	0.0083	0.1299	0.0022	1.1948	0.0222	0.90	787	12	798	10
HAEU2-f	Core	16	145	88	0.61	1.63E-04	0.24%	0.0664	0.0092	0.1268	0.0022	1.1604	0.0227	0.88	769	12	782	11
HAEU2-f	Rim	18	169	101	0.59	2.66E-04	0.42%	0.0669	0.0083	0.1218	0.0023	1.1236	0.0231	0.91	741	13	765	11
SHEU1-a	Rim	24	217	252	1.16	8.90E-06	0.00%	0.0660	0.0051	0.1280	0.0025	1.1644	0.0236	0.97	776	14	784	11
SHEU1-b	Rim	8	68	16	0.23	1.41E-04	0.15%	0.0660	0.0098	0.1312	0.0021	1.1940	0.0222	0.85	795	12	798	10
SHEU1-d	Core	9	88	67	0.77	8.26E-06	0.00%	0.0674	0.0048	0.1215	0.0017	1.1293	0.0170	0.95	739	10	767	8
SHEU1-d	Rim	15	134	110	0.82	6.13E-06	0.00%	0.0666	0.0067	0.1295	0.0019	1.1885	0.0189	0.91	785	11	795	9
SHEU1-e	Core	11	108	118	1.09	5.02E-04	0.80%	0.0641	0.0298	0.1233	0.0028	1.0909	0.0406	0.60	750	16	749	20
SHEU1-e	Rim	15	141	137	0.97	5.68E-04	0.92%	0.0650	0.0573	0.1277	0.0022	1.1448	0.0685	0.29	775	13	775	32
SHEU1-f	Core	12	101	89	0.87	1.06E-05	0.00%	0.0668	0.0093	0.1336	0.0024	1.2314	0.0245	0.88	809	13	815	11
SHEU1-f	Rim	13	97	83	0.86	5.07E-06	0.00%	0.0681	0.0176	0.1596	0.0056	1.4971	0.0591	0.90	954	31	929	24